

# 中天山、伊犁及塔里木地块开始参与 Rodinia 超大陆聚合过程早于新元古代?

蔡志慧,马绪宣,何碧竹

中国地质科学院地质研究所自然资源部深地动力学重点实验室,北京,100037

**内容提要:**长久以来,中国主要陆块被普遍认为比世界其他陆块开始参与罗迪尼亚超大陆聚合的时间较晚,为新元古代早期。为了探讨此问题,我们选择中国中天山、伊犁及塔里木地块作为主要研究对象,系统分析了新元古代早期( $1.0 \sim 0.8$  Ga)的构造变形及岩浆特征。新元古代早期构造变形主要表现为拉伸线理近平行于造山带方向,反映了后造山陆内走滑剪切过程。 $1.0 \sim 0.8$  Ga 的岩浆岩皆为较小规模花岗岩,未见基性包体,矿物组合中基本无角闪石,具有高钾钙碱性和过铝质特征,并含有大量捕获老锆石,说明古老基底或重熔地壳的显著参与。岩石源区主要为重熔基性下地壳,在构造背景判别图上基本落在后造山环境。锆石 Ti 及全岩 Zr 温度计算结果显示这些岩体的结晶温度普遍偏高,约  $800^{\circ}\text{C}$ 。结合已有区域地质资料,我们认为:①在新元古代原塔里木陆块(包括早期中天山、伊犁及塔里木地块)已经位于罗迪尼亚超大陆内部, $1.0 \sim 0.8$  Ga 变形及岩浆记录皆反映了原塔里木陆块与其它陆块碰撞后的构造事件;②由于超大陆聚合后的热毯效应使得新元古代早期花岗岩结晶温度偏高;③中天山、伊犁及现今塔里木地块最初参与罗迪尼亚超大陆汇聚的时间应早于新元古代( $>1.0$  Ga)。

**关键词:**新元古代;罗迪尼亚超大陆;中天山;伊犁;塔里木

多期超大陆重建是近年来地球历史研究的突出进展之一。目前公认的超大陆包括古元古-中元古代早期的哥伦比亚(Columbia,也称 Nuna)超大陆(Rogers et al., 2003, 2009; Meert, 2012; Evans, 2013)、中-新元古代的罗迪尼亚(Rodinia)超大陆(Powell et al., 1993, 2002; Hoffman 1992; Hoffman et al., 1998, 2011; Weil et al., 1998; Li ZX et al., 2008)以及晚古生代的潘吉亚(Pangea)超大陆(Rogers et al., 2003)等等。大量研究表明中国的主要陆块,如华北、华南以及塔里木克陆块都曾经参与了多期超大陆的聚合与离散过程(Li Zhengxiang et al., 1995, 2002; Li ZX, 2008; Zhao Guochun et al., 2003; Zhu Wenbin et al., 2008; Ge Rongfeng et al., 2015, 2016; Yao Jinlong et al., 2016; Wu Hailin et al., 2019)。在哥伦比亚、罗迪尼亚以及潘吉亚这三期超大陆旋回演化事件中,由于①哥伦比亚超大陆距今较远,有关

超大陆演化事件的证据相对较少,②潘吉亚超大陆解体时间距今较近,环境、古生物及岩石学等方面证据比较充分,研究者对其重建模型有较统一的认识,③罗迪尼亚超大陆的聚合与离散事件有一定的地质记录,但存在较多争议,并且其聚散过程伴随着古气候突变(Kirschvink, 1992)以及复杂生命的出现(McMenamin et al., 1990),故而罗迪尼亚超大陆形成演化过程引起了全球地学家的更广泛关注。

世界大部分地区陆块参与罗迪尼亚超大陆初始聚合过程主要发生在  $1.3 \sim 1.1$  Ga(格林威尔 Grenville 造山期)(如 Moores, 1991; Gose et al., 1997; Anderson et al., 1995; Condie, 1998; Bruguier et al., 1999; Jacobs et al., 2003; Berry et al., 2005),然而中国主要陆块参与罗迪尼亚超大陆聚合的时间被认为较晚,为  $1.0 \sim 0.8$  Ga,比全球主要陆块参与罗迪尼亚聚合的时间晚了  $0.3$  Ga。这一时间差是如何造成的?已有岩浆岩及同位素年

注:本文为中国自然科学基金项目(编号 41502198、41872121 及 41302166)、博士后科学基金项目(编号 2015M571083、2016T90122)、中国地质科学院基本科研业务项目(编号 JYYWF20180903、JYYWF20182103)及中国地质调查局地调地质调查项目(编号:DD20190060 及 DD20190006)联合资助成果。

收稿日期:2019-07-06;改回日期:2019-08-31;网络发表日期:2019-09-12;责任编辑:黄敏。

作者简介:蔡志慧,女,1980 年生。副研究员,构造地质学专业。Email: cai-zihui@hotmail.com。

引用本文:蔡志慧,马绪宣,何碧竹. 2019. 中天山、伊犁及塔里木地块开始参与罗迪尼亚超大陆聚合过程早于新元古代?. 地质学报, 93(10):2426~2445, doi: 10.19762/j.cnki.dizhixuebao.2019244.

Cai Zihui, Ma Xuxuan, He Bihu. 2019. The initial assembly of the Chinese Central Tianshan, Yili and Tarim blocks to the Rodinia supercontinent prior to the Early Neoproterozoic?. Acta Geologica Sinica, 93(10):2426~2445.

代研究结果证实中国主要陆块参与罗迪尼亞超大陸聚合的证据是否合理? 超大陸的形成过程包括从早期的洋-陸俯冲到后期的陸-陸碰撞是一个长期过程 (Bogdanova et al., 2009), 中国主要陆块中的 1.0 ~ 0.8 Ga 构造热事件是否说明它们只是记录了罗迪尼亞超大陸晚期聚合过程?

我们选择中天山、伊犁地块以及塔里木地块北缘作为典例来讨论以上科学问题。选定三者的原因如下:①中天山、伊犁地块以及塔里木地块北缘有着相对完整的前寒武纪地层与地质事件记录;②在前寒武纪时中天山、伊犁地块及现今塔里木地块都曾为原塔里木陆块的一部分, 直到新元古代晚期-古生代早期才从塔里木裂解出来, 通过对三者研究能帮助我们揭示原塔里木陆块参与罗迪尼亞超大陸聚合的过程;③前人在中天山、伊犁地块以及塔里木地块北缘做过较充分年代学及地球化学工作, 为我们收集数据提供便利。

## 1 大地构造背景

天山造山带和塔里木地块为中国西北部两个主要地质单元。天山造山带实为中亚造山带南缘。中

亚造山带为欧亚大陆中部最显著的显生宙增生造山带, 其被夹持于北部西伯利亚克拉通和南部华北及塔里木块地之间, 由若干缝合带及微陆块组成(例如 Jahn Borming, 2004; Kröner et al., 2007; Windley et al., 2007; Xiao Wenjiao et al., 2010) (图 1)。中天山地块及伊犁地块皆为中亚造山带中的微陆块, 二者又被看做为天山造山带的主要组成部分。中国天山造山带由北向南可分为北天山、中天山地块、伊犁地块和南天山几个构造单元(图 1)。北天山主要出露一套晚石炭世火山-沉积岩, 代表晚古生代的弧岩浆作用(Charvet et al., 2007; Xiao Wenjiao et al., 2010; Chen Xijie et al., 2013)。南天山岩石组合主要为晚寒武世-奥陶纪的沉积岩单元(砂岩、泥岩和灰岩)及少量火山岩夹层。中天山地块南缘为巴伦台断裂及中天山南缘断裂, 北缘为中天山北缘断裂以及沿其分布的科克苏-那拉提-冰达坂-米什沟-干沟-尾亚蛇绿混杂岩带(图 1)(Shu Liangshu et al., 2000, 2002)。中天山地块岩石组合可以分为前寒武纪基底以及南华纪-震旦纪-古生代火山-沉积盖层。伊犁地块与中天山地块具有非常相近的基底岩石组合(图 2)。研究表明前寒武纪

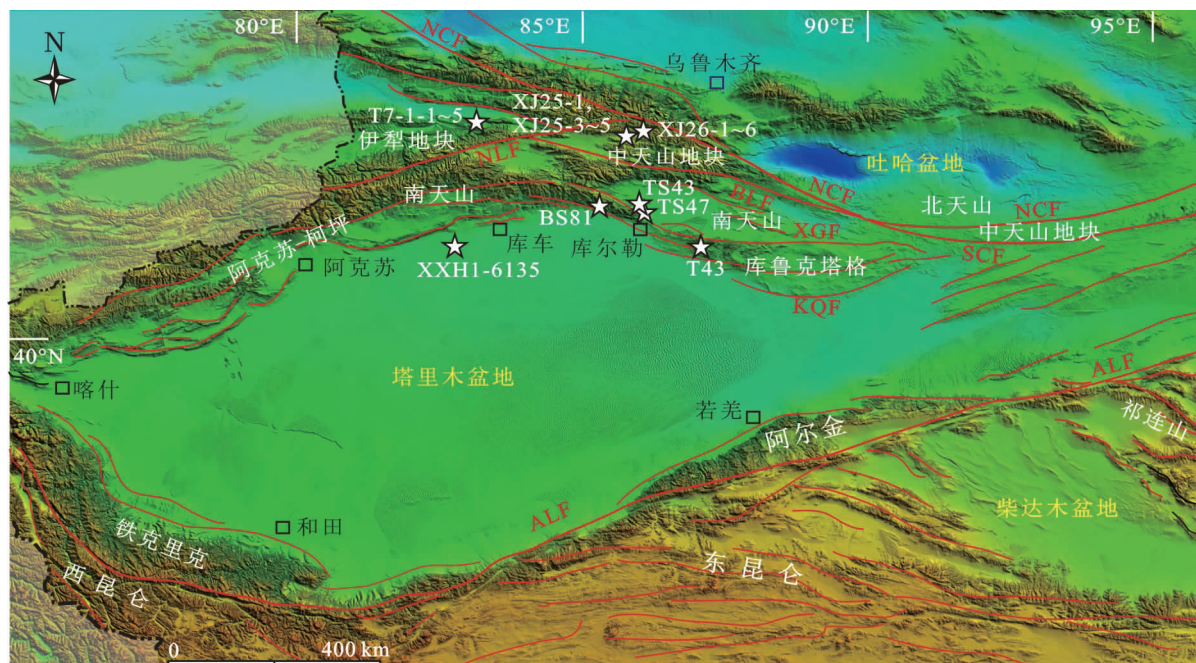


图 1 中天山、伊犁及塔里木地块构造简图及本文采样位置(根据 Xu Zhiqin et al., 2013 修改)

Fig. 1 A sketch structural map of the Central Tianshan, Yili and Tarim blocks

(modified after Xu Zhiqin et al., 2013) showing the locations of samples in this study

ALF—阿尔金断裂; BLF—巴伦台断裂; KQF—孔雀河断裂; NCF—中天山北缘断裂;

NLF—那拉提断裂; SCF—中天山南缘断裂; XGF—辛格尔断裂

ALF—Altun Fault; BLF—Baluntai Fault; KQF—Kongquehe Fault; NCF—Northern Central Tianshan Fault;

NLF—Nalati Fault; SCF—Southern Central Tianshan Fault; XGF—Xiger Fault

时中天山地块、伊犁及塔里木地块曾相邻并同属于罗迪尼亞超大陸(Shu Liangshu et al., 2000; Wang Bo et al., 2014a; Zuza et al., 2017)。新元古代晚期-古生代早期中天山和伊犁地块从原塔里木板块裂解出来的(Shu Liangshu et al., 1998)。早奥陶世,北天山洋(或古亚洲洋)洋壳沿 E-W 走向的尾亚-阿奇克库都格断裂带向塔里木板块北缘俯冲,形成中天山火山岛弧和南天山弧后边缘海盆(Shu Liangshu et al., 1998; Ge Rongfeng et al., 2012; Ma Xuxuan et al., 2014a)。二叠纪时北天山洋和南天山洋逐渐闭合,塔里木地块与中天山、伊犁地块再次拼合,塔里木地块与中亚造山带完成汇聚(Charvet et al., 2007, 2011; Yin Jiyuan et al., 2010; Dong Yumpeng et al., 2011; Han Baofu et al., 2011; Shu Liangshu et al., 2011; Ma Xuxuan et al., 2015; Huang He et al., 2019)。中天山与伊犁地块前寒武基底主要由中元古代低级变沉积岩以及变火山岩组成,并且被新元古花岗岩侵位(图 2)(Hu Aiqin et al., 2010; Chen Yibing et al., 1999, 2000; Liu Shuwen et al., 2004; Wang Zhongmei et al., 2014; Ma Xuxuan et al., 2014b; Chen Xinyue et al., 2009; Gao Jun et al., 2015, Li Ting et al., 2015)。Sm-Nd 和锆石 U-Pb 同位素研究表明在中天山和伊犁地块中可能存在古元古代或更老地壳(Hu Aiqin et al., 2000; Li Qiugen et al., 2003; Liu Shuwen et al., 2004; Huang Hu et al., 2019)。中天山南缘乌瓦门西石膏矿附近存在 2.5 Ga 的片麻岩,并叠加了 1.8 Ga 的角闪岩相变质作用(Wang Xinshui et al., 2017)。而同属于伊犁地块的哈萨克斯坦南部具有 2.8 Ga 的太古宙岩浆记录(Kröner et al., 2007)。

塔里木地块主要由中部面积大于 56 万平方公里的塔里木盆地及周缘盆山结合带(东北部库鲁克塔格、西北部阿克苏-柯坪、西南部铁克里克及东南部阿尔金地区)组成(图 1)。塔里木地块前寒武结晶基底与中天山和伊犁地块非常相似,也具有古老太古宙陆核,古元古代岩浆岩侵入其中(Hu Aiqin et al., 2006; Lu Songnian et al., 2008; Ge Rongfeng et al., 2013; Long Xiaoping et al., 2010, 2011; Ma Xuxuan et al., 2012; Zhang Chuanlin et al., 2012, 2013; Lu Songnian et al., 2008; Shu L S et al., 2011)。库鲁克塔格、铁克里克及塔里木盆地等塔里木地块内部地区广泛分布的 2.1~1.8 Ga 变质-岩浆岩被认为与哥伦比亚大陆

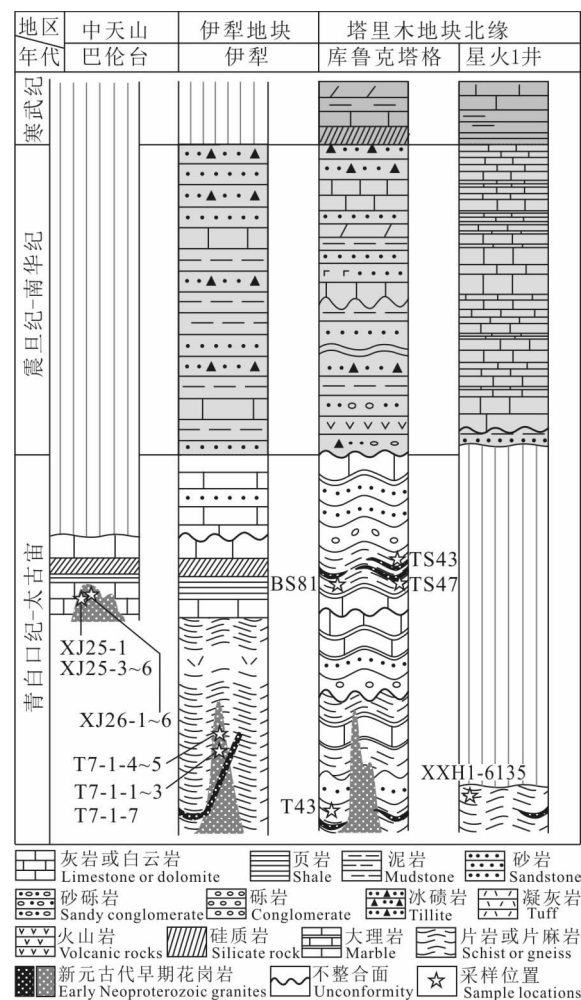


图 2 巴伦台、伊犁南部、库鲁克塔格及星火 1 井岩性柱状简图和采样位置

Fig. 2 Simplified lithologic column of the Baluntai, southern Yili, Kuluketage and Xinghuo-1 drilling well and sample locations

形成有关(Zhang Chuanlin et al., 2007; Shu L S et al., 2011; Xu Zhiqin et al., 2013; Ge Rongfeng et al., 2013; Wang Chao et al., 2014)。塔里木 1.75 Ma 岩浆记录被认为与哥伦比亚大陆大陆裂解有关(He Zhenyu et al., 2013; Yu Shengyao et al., 2013)。然而新元古代的变质-岩浆记录较复杂。1.0~0.8 Ga 的长英质岩浆岩主要分布在塔里木地块边缘(Zhang Chuanlin et al., 2006; Lu Songnian et al., 2008; Xu Zhiqin et al., 2013; Long Xiaoping et al., 2011; Shu L S et al., 2011; Wang Chao et al., 2015; Wu Guanghui et al., 2018),塔里木盆地中心的塔参 1 井岩心显示此位置具有多期次前寒武岩浆岩: 891~933 Ma、1195~1197 Ma 闪长岩-花岗闪长岩(Li Yuejun et al., 2003)以及 744

~790 Ma 的闪长岩-花岗闪长岩 (Guo Zhaojie et al., 2005)。

总体而言,由于中天山、伊犁及塔里木地块曾同属于罗迪尼亞超大陸(Shu Liangshu et al., 2000; Wang Bo et al., 2014a; Zuza et al., 2017),其新元古代岩漿岩具有相似之處。从形成時間上可將這些新元古代岩漿岩以分为二期:①早期岩漿(1.0~0.8 Ga)(Chen Yibing et al., 1999; Lu Songnian et al., 2008; Hu Aiqin et al., 2010; Shu L S et al., 2011; Zhang Chuanlin et al., 2012; Hu Aiqin et al., 2010; Li Ting et al., 2015; Wang Zhongmei et al., 2014; Gao Jun et al., 2015; Huang Zongying et al., 2015, 2017; Zhang Chuanlin. et al., 2007; Long Xiaoping et al., 2011; Wang Bo et al., 2014a, 2014b; Wu Guanghui et al., 2018)和②新元古代晚期(0.8~0.6 Ga)A 型花崗岩、少量闪长岩(Guo Zhaojie et al., 2005; Zhang Chuanlin et al., 2007; Lei Ruxiong et al., 2013)以及大量基性岩牆群及基性杂岩体(Xu Bei et al., 2005; Lu Songnian et al., 2008; Zhang Chuanlin et al., 2007)。其中新元古晚期岩漿作用被认为与罗迪尼亞超大陸裂解過程有关(Lu Songnian et al., 2008; Zhao Guochun et al., 2003; Zhao Guochun et al., 2012)。有关新元古代早期岩漿被解释为地壳部分熔融产物(Chen Yibing et al., 1999; Hu Aiqin et al., 2010; Long Xiaoping et al., 2011),但有关其与罗迪尼亞超大陸之间的关系讨论较少。另外有关中天山、伊犁及塔里木地块的新元古代地质事件研究主要集中在岩漿岩方面,相关的构造变形研究非常匮乏。本文将从中天山、伊犁及塔里木地块北緣的新元古代构造变形及岩漿特征入手,结合区域地质资料,综合讨论在罗迪尼亞超大陸聚合时三者的演化过程。

## 2 中天山、伊犁及塔里木陆块新元古构造变形特征

中天山、伊犁及塔里木地块前寒武结晶基底岩石与沉积盖层变形特征有明显差别(图 2)。中天山与伊犁地块规模较小,并且位于天山造山带内部,明显受到显生宙天山造山作用影响。岩石普遍叠加古生代以来构造变形记录(如 Wang Bo et al., 2010)。塔里木地块边缘如库鲁克塔格北部等距离造山带较近的地区也普遍受到显生宙构造影响。但通过变形期次划分我们可以识别出新元古代构造变形痕迹。

塔里木地块内部地区地震以及岩心钻井资料显示塔里木南华系盖层变形很弱,而基底变形较明显,表明这些变形形成时代为前南华纪。

中天山地块很多位置岩石发生明显变形。变形岩石中“S-C”组构及长石变斑晶、不对称褶皱等指示了中天山地块南緣和北緣皆具有右行剪切特征。本文中天山冰达坂样品 XJ25-1 与 XJ26-2 花崗岩也明显面理化(图 3a)。但如中天山地块其他地区岩石一样,其变形主要发生在古生代。

伊犁地块南部特克斯达根别里地区岩石类型主要包括变沉积岩与达根别里岩体。达根别里岩体为复合岩体,主要记录两期岩漿事件。第一期表现为灰白色花崗片麻岩,其侵入在元古宙变沉积岩中,具有强烈面理(面理产状为  $295^{\circ} \angle 58^{\circ}$ )(岩漿结晶时代为 930 Ma,本文)。第二期花崗岩为肉红色岩牆,无明显变形,并且穿切第一期花崗岩以及变沉积岩的面理(图 3b)。Xiong Fuhao et al. (2019)获得本文样品点附近的花崗岩牆锆石 U-Pb 年龄为 889 Ma。虽然伊犁地块南部很多地区受到古生代造山作用影响(Wang Bo et al., 2010),但灰白色花崗片麻岩的原岩花崗岩与肉红色花崗岩的成分略有差异,变形程度迥异,最可能的原因是 930 Ma 的灰白色花崗片麻岩中的构造最初形成时间早于 889 Ma 而古生代构造对此处影响不大。

塔里木地块北緣库魯克塔格西部和库爾勒地区多处显示新元古代混合岩化及变形现象(Deng Xingliang et al., 2008; Ge Rongfeng et al., 2013)。库魯克塔格附近前寒武基底岩石发生明显变形。至少可分为二期塑性变形。第一期变形表现为轴面近直立的褶皱,代表了最初的地壳增厚,我们未能对此期变形时间进行限定。第二期变形主要表现为沿兴地断裂普遍发育糜棱岩。这些糜棱岩面理走向近 E-W 向,呈中等-较高倾角倾向近 N 向,局部向 S 陡倾(图 3c),拉伸线理沿近 E-W 分布,平行于造山带方向。显微镜下黑云母石英片岩石英呈“σ”形,黑云母呈鱼状,指示右行剪切方向(图 4a、b)。未变形细晶花崗岩牆侵入这些变形岩石中。Deng Xingliang et al. (2008)获得此处侵入变形片麻岩中的细晶花崗岩牆 U-Pb 年龄为 798 Ma,说明变形时代早于 798 Ma。而兴地断裂南北两侧新元古代之前的地层特征并无明显区别,直到南华纪(0.8~0.68 Ga)时南北两侧地层厚度呈现明显差异(Sun Xiaomeng et al., 2006),说明兴地断裂最初形成应在南华纪,与其相关的糜棱岩应近似于或略

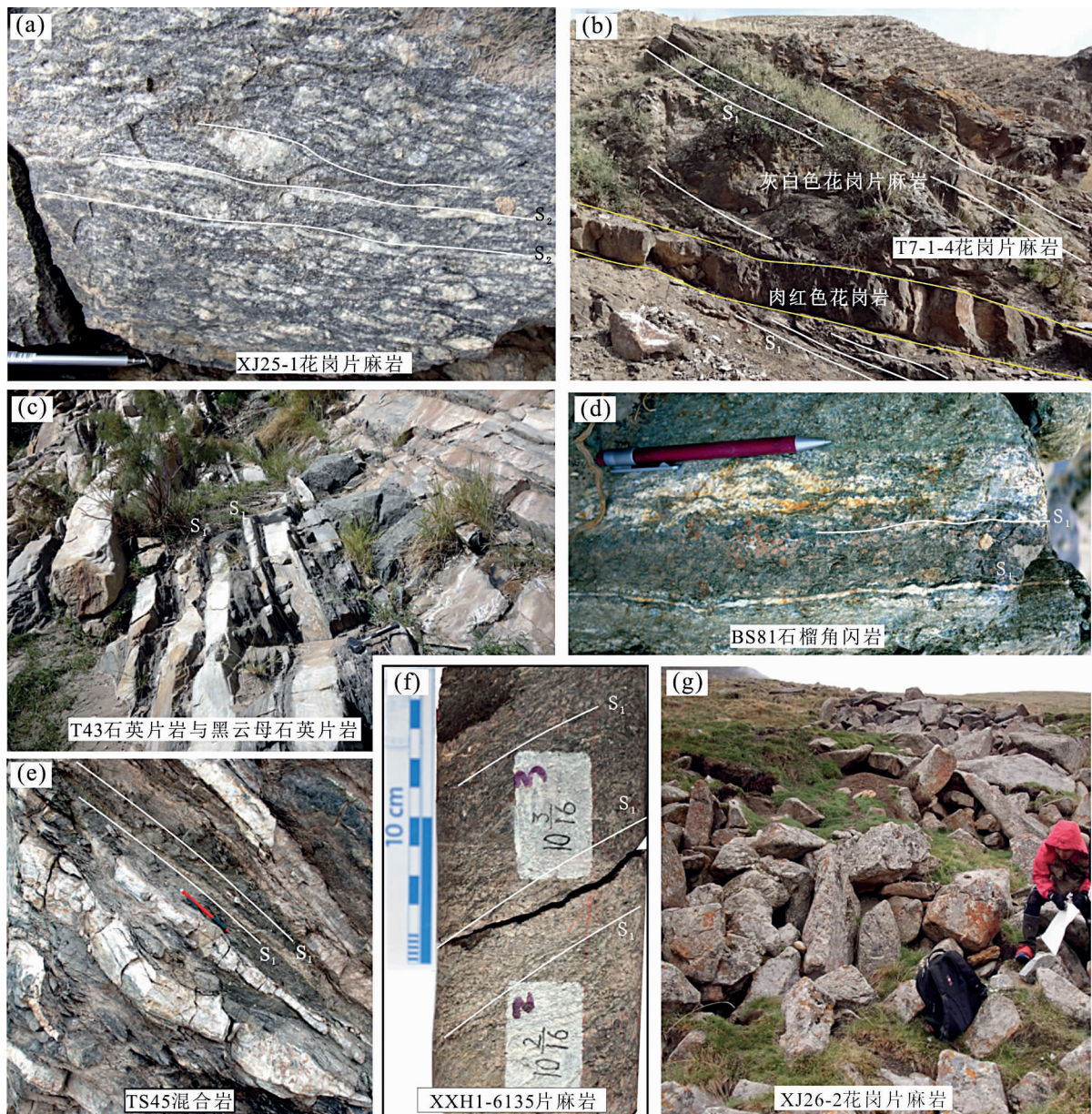


图 3 中天山、伊犁及塔里木地区新元古代早期变形现象及花岗片麻岩野外照片

Fig. 3 Field photos for the Neoproterozoic deformation features and granitic gneisses in the Central Tianshan, Yili and Tarim regions

$S_1$ —新元古面理;  $S_2$ —古生代面理

$S_1$ —Neoproterozoic foliation;  $S_2$ —Paleozoic foliation

早于兴地断裂形成时间。与此构造事件同期的细晶花岗岩墙(798 Ma, Deng Xingliang et al., 2008)很可能与兴地断裂形成有关。故而库鲁克塔兴地附近糜棱岩变形时间可限定为近似并略早于 798 Ma。

塔里木地块北部库尔勒地区普遍发育混合岩(图 3d,c)。这些混合岩多数向 S 或 SSW 方向呈中等高角度倾斜, 库尔勒西侧 29 团附近岩石向 N 陡倾。拉伸线理沿近 WNW-ESE 方向分布, 近平行于造山带方向(图 3c)。库尔勒混合岩的锆石 U-Pb 测

年结果显示, 混合岩形成时代为 830 Ma (Ge Rongfeng et al., 2013)。野外及显微镜下观察结果显示大多数库尔勒混合岩没有明显叠加后期变形。如深色体中的变形黑云母成分较一致, 反映岩石经历的主要一期变质变形时代应为 830 Ma。

我们采集了塔里木盆地北部星火 1 井中的结晶基底样品 XXH1-6135(采样深度为 6135m)。岩心样品显示其主要由长石+石英+白云母+黑云母组成, 发生明显变形, 面理倾角 40°(图 3f)。锆石 U-

Pb 测试结果为 832 Ma, 代表其岩浆结晶时代 (Xu Zhiqin et al., 2013)。白云母 Ar-Ar 年龄为 770 Ma(据作者未发表资料)代表冷却时代, 说明其变质变形时间早于 770 Ma。另外根据星火 1 井、地球物理及钻井资料可知其上部震旦系盖层未发生变形(图 2), 也可将基底变形时代限定为早于震旦纪。

### 3 中天山、伊犁及塔里木地块的早新元古代岩浆岩

#### 3.1 样品采集与描述

本文岩浆岩样品采自中天山地块冰达坂地区和伊犁地块特克斯西达根别里地区。冰达坂样品 XJ25-1、XJ25-3~6 和 XJ26-1~6 皆为花岗片麻岩(图 3a,g), 主要由斜长石、钾长石、黑云母和石英组成, 发育有面理及褶皱等后期韧性变形构造(图

3a)。达根别里样品 T7-1-1~5 及 T7-1-7 花岗片麻岩整体呈灰白色, 面理化, 由钾长石、石英、黑云母和斜长石组成, 显微镜下见蠕英结构(图 4)。

#### 3.2 分析方法

为了更好地讨论新元古早期岩浆岩大地构造意义我们对样品 XJ25-1、XJ26-2 和 T7-1-4 进行了锆石 U-Pb 定年、锆石微量元素测试以及全岩地球化学成分分析。在进行锆石 U-Pb 定年和微量元素测试之前我们对样品进行预处理。将分选出来的锆石用环氧树脂固定并固化, 接着对其表面进行剖光至锆石内部暴露, 然后进行锆石阴极发光图像特征分析。U-Pb 同位素定年和微量元素含量在武汉上谱分析科技有限责任公司利用 LA-ICP-MS 同时分析完成。详细的仪器参数和分析流程见 Zong Keqing et al. (2017)。GeolasPro 激光剥蚀系统由

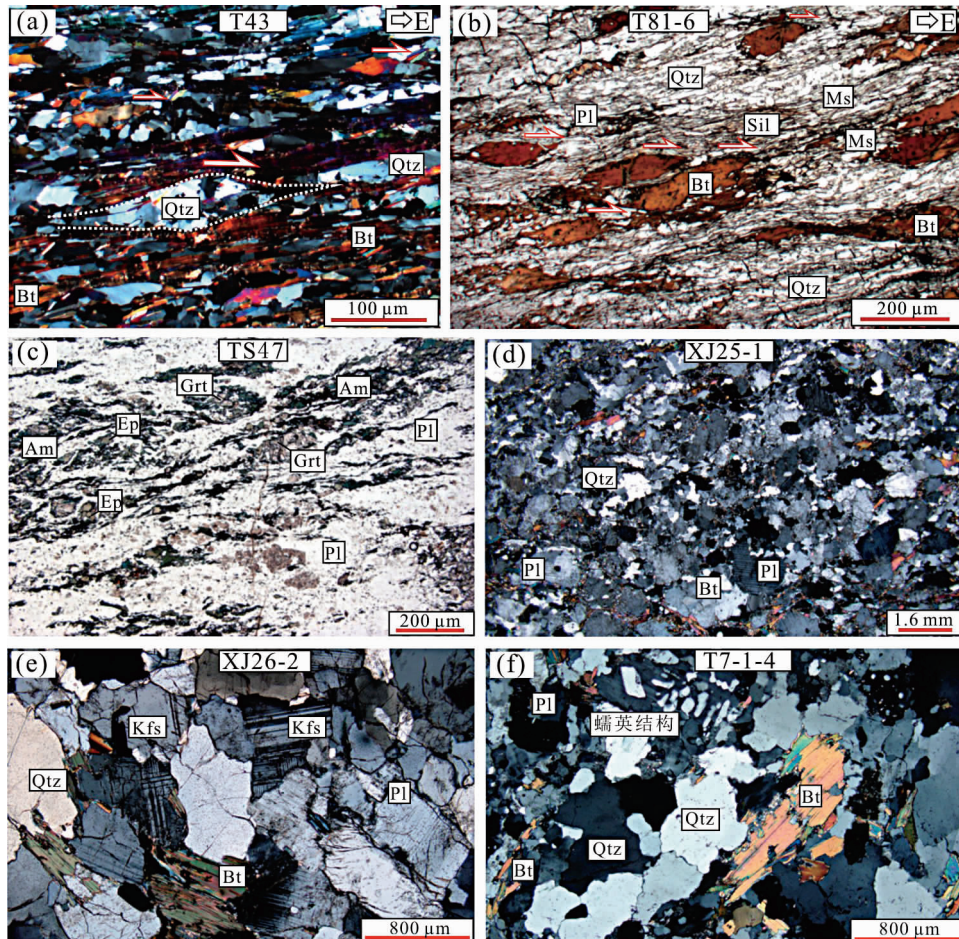


图 4 (a~c) 塔里木地块北缘新元古代变形岩石; (d~e) 中天山和伊犁地块新元古代早期花岗片麻岩显微照片

Fig. 4 (a~c) Photomicrographs for the Neoproterozoic deformed rocks on the northern margin of the Tarim Block;

(d~e) Photomicrographs for the Neoproterozoic granites in the Chinese Central Tianshan and Yili blocks

Bt—黑云母, Ep—绿帘石, Grt—石榴子石; Kfs—钾长石, Ms—白云母, Pl—斜长石, Qtz—石英, Sil—矽线石

Am—amphibole; Bt—biotite; Ms—muscovite; Sil—silicalite; Qtz—quartz; Grt—garnet; Pl—plagioclase;

Kf—potassium feldspar; Ep—epidote

COMPExPro 102 ArF 193 nm 准分子激光器和 MicroLas 光学系统组成, ICP-MS 型号为 Agilent 7700e。激光剥蚀过程中采用氦气作载气、氩气为补偿气以调节灵敏度,二者在进入 ICP 之前通过一个 T 型接头混合,激光剥蚀系统配置有信号平滑装置 (Hu Zhaochu et al., 2015)。本次分析的激光束斑和频率分别为 44 μm。U-Pb 同位素定年和微量元素含量处理中采用锆石标准 91500 和玻璃标准物质 NIST610 作外标分别进行同位素和微量元素分馏校正。每个时间分辨分析数据包括大约 20-30 s 空白信号和 50 s 样品信号。数据处理(包括对样品和空白信号的选择、仪器灵敏度漂移校正、元素含量及 U-Pb 同位素比值和年龄计算)采用软件 ICPMSDataCal(Liu Yongsheng et al., 2010)完成。锆石 U-Pb 年龄谐和图绘制和加权平均年龄计算采用 Isoplot/Ex\_ver3(Ludwig, 2003)完成。全岩主、微量元素和稀土元素分析在广州澳实科技检测分析有限公司完成。主量元素采用 X-射线荧光融片法进行含量测定,所选仪器为 ME-XRF26d。微量元素和稀土元素分析采用电感耦合等离子质谱仪 (ME-ICP61 和 ME-MS81) 进行。微量元素分析精度优于 5%。具体操作方法和原理详见 Liu Ying et al. (1996)。

### 3.3 分析结果

#### 3.3.1 岩体结晶年龄

我们分别对中天山冰达坂和伊犁达根别里岩体的锆石进行同位素 U-Pb 定年。测试结果显示这些锆石具有较高的 Th/U 比值,普遍大于 0.1,主要介于 0.2~1.0 之间(表 1)。其阴极发光图像显示较好晶形及环带特征(图 5),说明这些锆石基本都是岩浆成因锆石,U-Pb 年龄代表岩体侵位的结晶时代。中天山冰达坂花岗片麻岩(XJ25-1)的锆石 U-Pb 年龄相对分散,有两颗较老的锆石显示 1448 Ma 和 1301 Ma。其他锆石的年龄则相对集中,谐和年龄为 929.5±3.2 Ma,代表岩体侵位时的结晶年龄(图 5a)。相似地,样品 XJ26-2 中的几颗锆石具有 1400~1500 Ma 的年龄。但其余大量锆石显示相对集中的年龄,对应的加权平均年龄为 928.7±4.3 Ma(图 7)。这一谐和年龄结果与样品 XJ25-1 的测年结果在误差范围内一致,进一步证明测试结果的准确性和可靠性,表明冰达坂南的这个片麻状花岗岩体的侵位时代约为 930 Ma。伊犁达根别里花岗片麻岩样品中的锆石年龄也大部分集中在 930 Ma 左右。仅 2 颗锆石具有 1020 Ma 左右的年龄。相

对集中的锆石给出的加权平均年龄为 929.7±5.3 Ma(图 8)。说明达根别里花岗岩体侵位时代为新元古代早期。所有锆石 U-Pb 测年结果见表 1。

#### 3.3.2 全岩地球化学成分特征

中天山冰达坂和伊犁达根别里的花岗岩全岩地球化学测试结果列于表 2。结合已发表的中天山、伊犁及塔里木地块北缘新元古代早期花岗岩地球化学数据,我们系统分析这些数据特征及其指示意义。

中天山、伊犁及塔里木地块北缘新元古代早期花岗岩主量元素特征显示如下,  $\text{SiO}_2 = 58.56\% \sim 77.75\%$  之间,  $\text{Al}_2\text{O}_3 = 11.16\% \sim 18.13\%$ ,  $\text{TiO}_2 = 0.01\% \sim 1.19\%$ ,  $\text{Na}_2\text{O} = 1.81\% \sim 8.24\%$ ,  $\text{K}_2\text{O} = 0.67 \sim 6.3\%$ ,  $\text{MgO} = 0.05\% \sim 2.95\%$ ,  $\text{CaO} = 0.32\% \sim 5.43\%$ (表 2)。这些新元古代早期岩浆岩  $\text{SiO}_2$  百分含量主要落在 65%~80% 区间,峰值为 72.6%(图 6a),为典型花岗岩类。在  $\text{K}_2\text{O}-\text{SiO}_2$  图解上,中天山、伊犁及塔里木地块北缘样品的分布范围较大,但主体落在高钾钙碱性到钾玄岩区间(图 6b)。在图 6c 中,这些新元古代早期的岩浆岩全部落在过铝质岩石区域。岩石稀土总量变化较大,多数为  $22 \times 10^{-6} \sim 760 \times 10^{-6}$ ,稀土元素配分图具有轻微的右倾型特征(本文及相关文献)(图 6d),二个样品为淡色体稀土总量为  $1.51 \sim 3.33 \times 10^{-6}$ ,稀土元素配分图轻微左倾(Wang Bo et al., 2014b)(图 6d)。

## 4 讨论

### 4.1 新元古代早期构造变形特征主要揭示原塔里木陆块后造山陆内走滑剪切过程

走滑剪切是陆-陆碰撞后的一种重要陆内物质运动方式(如新生代青藏高原, Tapponier et al., 2001)。在塔里木地块北缘及伊犁地块中都可见新元古代早期构造变形现象(图 3、图 4)。本文库鲁克塔格及库尔勒地区的岩石变形特征都指示了新元古代早期在原塔里木陆块(包括中天山、伊犁及现今塔里木地块等)北缘发生右行剪切过程(图 4)。说明新元古代早期(1.0~0.8 Ga)时原塔里木北缘已经进入陆内造山阶段。原塔里木陆块可能与某未知陆块碰撞后可能发生陆内斜向汇聚过程。发生在原塔里木陆块北部的洋-陆汇聚阶段变形并不明显或已被后期变形所置换,即原塔里木陆块参与罗迪尼亚汇聚的初始时间应早于 1.0 Ga,这与世界上其他地区所记录的罗迪尼亚最初汇聚时间一致。

表 1 中天山及伊犁地区样品 LA-ICP-MS 锆石 U-Pb 测年结果

Table 1 LA-ICP-MS zircon U-Pb dating results for samples from Central Tianshan and Yili regions

分析点	元素含量			比值			年龄 (Ma)			岩浆结晶温度(℃)						
	Th(× 10 <sup>-6</sup> )	U(× 10 <sup>-6</sup> )	Ti(× 10 <sup>-6</sup> )	Th/U	<sup>207</sup> Pb / <sup>206</sup> Pb	误差 1σ	<sup>207</sup> Pb / <sup>235</sup> Pb	误差 1σ	<sup>207</sup> Pb / <sup>206</sup> Pb	误差 1σ	<sup>206</sup> Pb / <sup>238</sup> Pb	误差 1σ	$T_a$	$T_b$		
	采样位置 43°01'22.78"N, 86°45'44.9"E															
样品 XJ25-1 采样位置: 43°01'22.78"N, 86°45'44.9"E																
XJ25-1-01	331	325	1.02	0.0887	0.0020	3.0888	0.0690	0.2520	0.0023	1398.5	44.4	1429.9	17.1	1448.5	11.7	
XJ25-1-02	1747	2217	16.31	0.79	0.0726	0.0027	1.5502	0.0568	0.1549	0.0038	1003.4	77.8	950.6	22.6	928.4	21.1
XJ25-1-03	643	4220	11.52	0.15	0.0705	0.0011	1.5116	0.0261	0.1549	0.0015	942.6	33.3	935.1	10.6	928.5	8.5
XJ25-1-04	1400	3225	2.09	0.43	0.0708	0.0017	1.5146	0.0379	0.1547	0.0025	951.5	48.6	936.3	15.3	927.1	13.7
XJ25-1-05	2703	4905	30.75	0.55	0.0736	0.0012	1.7270	0.0293	0.1699	0.0014	1031.5	33.3	1018.6	10.9	1011.5	7.7
XJ25-1-06	1408	4668	14.75	0.30	0.0714	0.0013	1.5312	0.0308	0.1551	0.0016	968.5	37.5	943.0	12.4	929.6	8.9
XJ25-1-07	747	3700	13.15	0.20	0.0715	0.0014	1.5311	0.0306	0.1548	0.0013	972.9	38.9	942.9	12.3	928.0	7.1
XJ25-1-08	765	2723	10.16	0.28	0.0710	0.0012	1.5202	0.0276	0.1547	0.0012	966.7	35.2	938.6	11.1	927.0	6.9
XJ25-1-09	629	3067	17.65	0.21	0.0708	0.0012	1.5222	0.0278	0.1553	0.0013	951.5	35.2	939.4	11.2	930.3	7.3
XJ25-1-10	3371	7140	0.47	0.0755	0.0013	1.6363	0.0362	0.1561	0.0021	1083.3	30.6	984.3	14.0	934.9	11.9	
XJ25-1-11	1192	3498	14.90	0.34	0.0697	0.0014	1.4958	0.0282	0.1548	0.0010	920.4	39.7	928.7	11.5	927.7	5.7
XJ25-1-12	492	1141	38.84	0.43	0.0705	0.0016	1.5157	0.0335	0.1547	0.0013	942.6	44.9	936.7	13.5	927.4	7.0
XJ25-1-13	237	362	0.65	0.0853	0.0022	2.6570	0.0733	0.2237	0.0025	1324.1	50.5	1316.6	20.4	1301.3	13.0	
XJ25-1-14	505	2620	11.12	0.19	0.0699	0.0013	1.5082	0.0310	0.1550	0.0014	925.6	38.9	933.7	12.6	929.0	8.0
XJ25-1-15	1398	4192	10.76	0.33	0.0717	0.0013	1.5441	0.0312	0.1550	0.0020	988.9	36.0	948.2	12.4	928.8	11.1
XJ25-1-16	992	4791	20.13	0.21	0.0700	0.0012	1.5114	0.0291	0.1555	0.0016	927.8	32.4	935.0	11.8	931.5	8.7
XJ25-1-17	456	2315	9.98	0.20	0.0719	0.0013	1.5446	0.0285	0.1548	0.0016	983.3	37.0	948.3	11.4	927.9	8.8
XJ25-1-18	557	2858	10.38	0.19	0.0702	0.0014	1.5128	0.0323	0.1551	0.0015	933.0	38.0	935.6	13.1	929.6	8.4
XJ25-1-19	3555	4948	21.91	0.72	0.0703	0.0015	1.5081	0.0426	0.1547	0.0035	936.7	44.4	933.7	17.2	927.3	19.4
XJ25-1-20	696	2792	16.00	0.25	0.0674	0.0012	1.4550	0.0264	0.1557	0.0014	850.0	38.1	912.0	10.9	932.6	7.7
XJ25-1-21	343	1260	26.75	0.27	0.0670	0.0013	1.4444	0.0279	0.1553	0.0012	838.9	40.7	907.5	11.6	930.7	6.7
XJ25-1-22	2341	2662	34.87	0.88	0.0691	0.0011	1.4907	0.0241	0.1553	0.0011	901.9	61.1	926.6	9.8	930.8	6.4
XJ25-1-23	2753	6882	26.54	0.40	0.0713	0.0013	1.5351	0.0274	0.1551	0.0015	965.7	41.7	944.6	11.0	929.4	8.6
XJ25-1-24	2782	4945	19.44	0.56	0.0686	0.0013	1.4797	0.0317	0.1551	0.0019	887.0	36.1	922.1	13.0	929.4	10.8
XJ25-1-25	1873	4872	18.21	0.38	0.0776	0.0017	1.6685	0.0384	0.1551	0.0021	1144.5	44.4	996.6	14.6	929.6	11.7
XJ25-1-26	1020	5903	21.78	0.17	0.0693	0.0013	1.4923	0.0317	0.1550	0.0020	907.1	34.3	927.3	12.9	928.9	11.0
XJ25-1-27	1370	3135	12.25	0.44	0.0701	0.0016	1.5091	0.0344	0.1550	0.0014	931.5	47.1	934.1	13.9	929.1	7.7
XJ25-1-28	708	3147	17.52	0.23	0.0703	0.0012	1.5169	0.0274	0.1553	0.0013	936.7	35.2	937.2	11.1	930.7	7.3
XJ25-1-29	675	2768	7.41	0.24	0.0682	0.0013	1.4669	0.0275	0.1550	0.0011	875.9	40.7	916.9	11.3	929.0	6.3
XJ25-1-30	870	5437	11.74	0.16	0.0688	0.0014	1.4839	0.0303	0.1554	0.0014	894.4	74.2	923.8	12.4	930.9	7.7
样品 XJ26-2 采样位置: 43°03'22.68"N, 86°47'3.68"E																
XJ26-2-01	993	4720	15.6	0.21	0.0700	0.0013	1.5120	0.0283	0.1553	0.0013	929.3	36.7	935.3	11.4	930.9	7.1
XJ26-2-02	731	2681	13.2	0.27	0.0702	0.0013	1.5087	0.0318	0.1548	0.0019	1000.0	37.0	933.9	12.9	927.7	10.7
XJ26-2-03	5420	8628	0.63	0.942	0.0014	3.4820	0.0585	0.2667	0.0027	1522.2	27.6	1523.1	13.3	1524.0	13.9	
XJ26-2-04	1838	3335	0.55	0.940	0.0015	3.4147	0.0692	0.2622	0.0035	1509.3	29.6	1507.8	15.9	1500.8	18.1	
XJ26-2-05	7392	8877	0.83	0.948	0.0015	3.4881	0.0588	0.2659	0.0018	1524.1	30.7	1524.5	13.3	1520.1	9.1	
XJ26-2-06	781	2187	7.0	0.36	0.0727	0.0015	1.5545	0.0330	0.1548	0.0012	1005.6	43.4	952.3	13.1	927.8	6.5

续表 1

分析点	元素含量				比值				年龄 (Ma)				岩浆结晶温度(℃)			
	Th(×10 <sup>-6</sup> )	U(×10 <sup>-6</sup> )	Ti(×10 <sup>-6</sup> )	Th/U	207Pb /206Pb	误差 1σ	207Pb /235Pb	误差 1σ	206Pb /238Pb	误差 1σ	207Pb /206Pb	误差 1σ	206Pb /238Pb	误差 1σ	T <sub>a</sub>	T <sub>b</sub>
XJ26-2-07	503	1864	6.4	0.27	0.0722	0.0015	1.5423	0.0328	0.1545	0.0012	992.3	41.5	947.4	13.1	926.1	6.7
XJ26-2-08	2638	5402	13.1	0.49	0.0733	0.0012	1.7227	0.0326	0.1702	0.0019	1033.3	34.4	1017.0	12.2	1013.0	10.4
XJ26-2-09	1472	3574	17.4	0.41	0.0711	0.0011	1.5201	0.0260	0.1545	0.0012	961.1	32.9	938.5	10.5	926.2	6.6
XJ26-2-10	1488	4607	0.32	0.0719	0.0011	1.5455	0.0275	0.1553	0.0015	984.3	31.5	948.7	11.0	930.8	8.2	
XJ26-2-11	3462	5806	0.60	0.0937	0.0014	3.3315	0.0554	0.2570	0.0022	1501.9	27.8	1488.5	13.0	1474.3	11.3	
XJ26-2-12	2376	4880	16.8	0.49	0.0700	0.0012	1.5029	0.0277	0.1552	0.0013	927.8	34.7	931.6	11.2	930.2	7.2
XJ26-2-13	1959	5456	10.5	0.36	0.0701	0.0012	1.5035	0.0289	0.1552	0.0017	931.5	35.2	931.8	11.7	929.8	9.4
XJ26-2-14	601	1913	3.5	0.31	0.0680	0.0013	1.4569	0.0277	0.1548	0.0010	869.4	38.9	912.7	11.5	927.7	5.5
XJ26-2-15	1142	3104	4.6	0.37	0.0704	0.0012	1.5078	0.0258	0.1548	0.0010	938.9	33.3	933.5	10.4	927.8	5.7
XJ26-2-16	297	618	0.48	0.0936	0.0016	3.3678	0.0622	0.2603	0.0024	1499.7	-0.9	1496.9	14.5	1491.2	12.2	
XJ26-2-17	620	2542	11.9	0.24	0.0699	0.0012	1.5022	0.0302	0.1553	0.0016	924.1	37.0	931.3	12.3	930.6	9.0
XJ26-2-18	280	3859	0.07	0.0868	0.0016	2.8228	0.0680	0.2344	0.0035	1366.7	35.0	1361.6	18.1	1357.4	18.5	
XJ26-2-19	2458	9748	5.3	0.25	0.0707	0.0012	1.5150	0.0281	0.1549	0.0014	950.0	32.4	936.5	11.4	928.5	7.9
XJ26-2-20	2944	4187	0.70	0.0937	0.0015	3.3928	0.0611	0.2619	0.0025	1501.9	30.7	1502.7	14.1	1499.3	12.9	
XJ26-2-21	3211	6204	16.0	0.52	0.0719	0.0012	1.5448	0.0274	0.1552	0.0014	983.3	33.3	948.4	10.9	930.1	7.9
XJ26-2-22	1647	3397	0.48	0.0917	0.0016	3.1016	0.0550	0.2445	0.0020	1461.1	33.2	1433.1	13.6	1410.1	10.4	
XJ26-2-23	1265	1811	0.70	0.0976	0.0021	3.1092	0.0656	0.2303	0.0018	1588.9	40.7	1435.0	16.2	1336.0	9.5	
XJ26-2-24	528	1008	0.52	0.0948	0.0025	3.4170	0.0923	0.2603	0.0027	1524.1	48.1	1508.3	21.2	1491.3	14.0	
XJ26-2-25	1228	1774	0.69	0.0951	0.0023	3.1848	0.0764	0.2418	0.0022	1531.5	45.8	1453.5	18.5	1396.2	11.7	
XJ26-2-26	7704	5330	1.45	0.0781	0.0018	1.6661	0.0361	0.1553	0.0019	1150.0	44.4	995.7	13.7	930.8	10.5	
XJ26-2-27	1326	2081	0.64	0.0950	0.0019	3.5032	0.0738	0.2661	0.0027	1528.7	33.2	1527.9	16.6	1520.8	13.8	
XJ26-2-28	1743	4215	14.6	0.41	0.0738	0.0014	1.5877	0.0298	0.1553	0.0014	1038.9	38.9	965.4	11.7	930.5	7.7
XJ26-2-29	5012	6066	21.4	0.83	0.0716	0.0013	1.5433	0.0353	0.1553	0.0024	975.9	37.0	947.8	14.1	930.4	13.3
XJ26-2-30	1004	3522	8.6	0.29	0.0698	0.0014	1.5011	0.0297	0.1553	0.0012	920.4	42.6	930.8	12.1	930.7	6.6
样品 T <sub>7-1-4</sub> 采样位置: 43°10'11"N, 82°12'00"E																
T7-1-4-01	30	265	0.12	0.0729	0.0005	1.5701	0.0199	0.1561	0.0016	1013.0	17.6	958.5	7.9	935.1	8.6	
T7-1-4-03	49	232	0.21	0.0747	0.0006	1.7462	0.0180	0.1695	0.0013	1061.1	10.2	1025.8	6.6	1009.5	7.1	
T7-1-4-04	499	548	0.91	0.0720	0.0005	1.5313	0.0171	0.1541	0.0010	987.0	19.4	943.0	6.9	923.9	5.7	
T7-1-4-05	299	301	0.99	0.0723	0.0009	1.5411	0.0257	0.1545	0.0010	994.4	25.9	946.9	10.3	926.4	5.7	
T7-1-4-06	43	295	0.15	0.0713	0.0009	1.5451	0.0197	0.1572	0.0012	966.4	24.5	948.6	7.8	941.4	6.6	
T7-1-4-08	18	286	0.06	0.0705	0.0011	1.5140	0.0363	0.1560	0.0036	942.6	33.3	936.1	14.7	934.5	20.3	
T7-1-4-10	21	219	0.09	0.0717	0.0005	1.5374	0.0157	0.1554	0.0012	988.9	13.4	945.5	6.3	931.4	6.9	
T7-1-4-12	43	467	0.09	0.0698	0.0018	1.4645	0.0453	0.1520	0.0009	924.1	51.9	915.9	18.7	912.3	5.2	
T7-1-4-13	462	530	0.87	0.0747	0.0011	1.5961	0.0161	0.1561	0.0021	1061.1	30.1	968.7	6.3	935.0	11.8	
T7-1-4-14	266	328	0.81	0.0736	0.0004	1.5900	0.0150	0.1568	0.0014	1031.5	9.3	966.3	5.9	938.8	8.0	
T7-1-4-15	13	286	0.05	0.0715	0.0003	1.5242	0.0091	0.1545	0.0007	972.2	12.0	940.2	3.7	926.4	4.1	
T7-1-4-16	29	296	0.10	0.0709	0.0004	1.5202	0.0185	0.1553	0.0013	955.2	13.0	938.6	7.4	930.8	7.5	
T7-1-4-17	140	192	0.73	0.0790	0.0008	1.8520	0.0304	0.1698	0.0018	1172.2	20.4	1064.2	10.8	1011.0	9.7	
T7-1-4-19	59	245	0.24	0.0717	0.0003	1.5490	0.0102	0.1566	0.0007	976.9	9.3	950.1	4.1	938.1	4.0	
T7-1-4-20	12	175	0.07	0.0711	0.0014	1.5138	0.0638	0.1540	0.0037	961.1	45.4	936.0	25.8	923.3	20.9	

注: 岩浆结晶温度 T<sub>a</sub> 和 T<sub>b</sub> 分别根据 Watson et al. (2006) 和 Ferry et al. (2007) 的 Ti 在锆石中温度计方法计算。

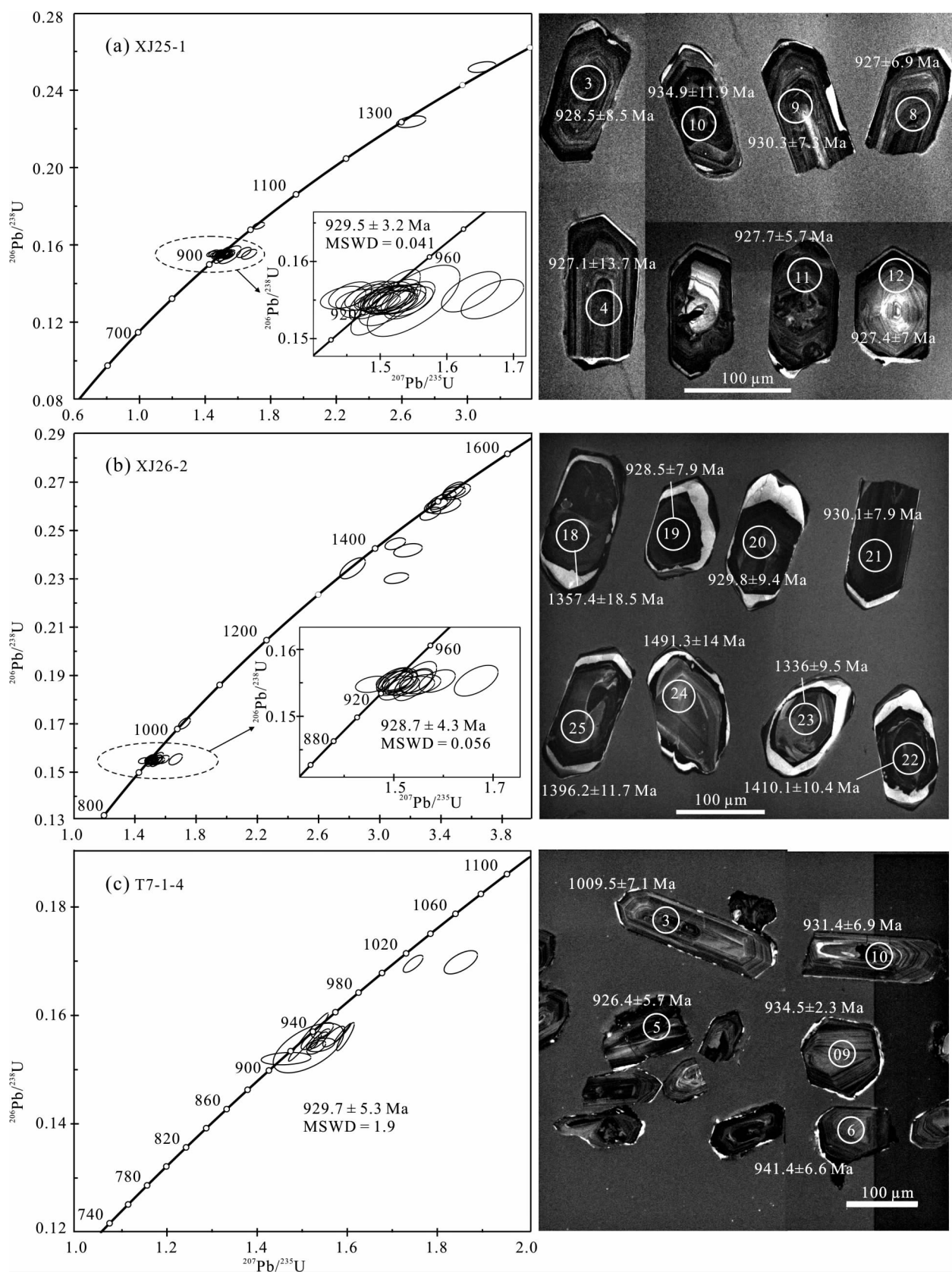


图 5 中天山及伊犁地区花岗片麻岩锆石 U-Pb 年龄谱和图及阴极发光照片

Fig. 5 Concordia diagram for the zircon U-Pb ages and representative CL images of the granitic gneisses from Central Tianshan and Yili regions

表 2 中天山和伊犁地区样品地球化学测试结果

Table 2 Geochemical data for the studied samples from Central Tianshan and Yili regions

样品	单位	XJ 25-3	XJ 25-4	XJ 25-5	XJ 25-6	XJ 26-1	XJ 26-2	XJ 26-3	XJ 26-4	XJ 26-5	XJ 26-6	T7-1-1	T7-1-2	T7-1-3	T7-1-7	T7-1-4	T7-1-5
SiO <sub>2</sub>	%	71.86	72.2	72.97	69.58	71.79	71.12	71.4	72.05	67.99	71.32	76.26	76.73	77.39	76.19	71.2	71.53
TiO <sub>2</sub>	%	0.44	0.27	0.25	0.4	0.3	0.36	0.31	0.3	0.39	0.31	0.07	0.05	0.06	0.07	0.41	0.24
Al <sub>2</sub> O <sub>3</sub>	%	13.48	14.58	13.9	15.12	15.16	15	15.07	15.2	16.86	15.62	12.6	12.38	12.42	12.62	13.59	14.32
TEFe <sub>2</sub> O <sub>3</sub>	%	2.89	2.22	2	2.98	2.32	2.74	2.38	2.26	3.36	2.42	1.09	0.78	0.86	1.10	2.59	1.64
MnO	%	0.08	0.04	0.03	0.06	0.04	0.04	0.04	0.04	0.08	0.04	0.02	0.02	0.02	0.02	0.06	0.04
MgO	%	0.68	0.41	0.39	0.93	0.73	0.88	0.78	0.79	1.06	0.8	0.15	0.13	0.13	0.16	1.01	0.57
CaO	%	2.86	1.56	1.55	2.28	3.47	3.49	3.48	3.3	4.45	3.73	0.64	1.1	0.73	0.65	2.19	1.61
Na <sub>2</sub> O	%	3.59	2.98	2.97	3.31	3.91	3.89	4.1	4.31	3.82	4.06	3.37	3.54	3.3	3.36	2.87	3.1
K <sub>2</sub> O	%	2.05	5.12	4.29	3.68	1.02	0.82	0.67	0.76	0.78	0.68	5.07	4.35	4.65	5.05	4.1	5.09
P <sub>2</sub> O <sub>5</sub>	%	0.09	0.06	0.05	0.12	0.04	0.06	0.06	0.07	0.13	0.07	0.02	0.02	0.02	0.02	0.13	0.06
LOI	%	1.14	0.81	0.71	1.38	0.71	0.86	0.98	1.09	0.98	1	0.48	0.79	0.52	0.44	0.77	0.91
总量	%	99.16	100.25	99.11	99.84	99.49	99.26	99.27	100.17	99.90	100.05	99.77	99.89	100.10	99.68	98.92	99.11
Rb	10 <sup>-6</sup>	90.2	210	176	153.5	60.4	45	33.5	30.6	33.5	26.3	366	377	365	374	224	237
Zr	10 <sup>-6</sup>	254	247	231	230	316	331	343	333	181	240	99.9	63.2	86.5	92.4	196	124
Y	10 <sup>-6</sup>	25	75.9	89.3	12.3	25.8	22	25.2	22.9	20.7	29.3	49.3	41.8	31.5	41.7	32.1	28.5
Nb	10 <sup>-6</sup>	12.9	10	9.5	13.2	8.9	10.1	9.3	9	7.1	9.2	11.8	10.2	11	11.6	11.7	9.29
La	10 <sup>-6</sup>	82.6	43	37	49.9	82.6	88.7	80.7	87.1	17.3	51.1	15	13.7	11.4	14.1	40.9	22.3
Ce	10 <sup>-6</sup>	156	87.4	76.2	90.7	156	169.5	156.5	167.5	35.4	100.5	33.8	33.4	28	31.4	79.3	44.2
Pr	10 <sup>-6</sup>	16.05	9.21	8.28	8.5	16.1	17.2	15.9	17.4	3.82	10.75	4.31	4.52	3.42	4.09	9.57	5.24
Nd	10 <sup>-6</sup>	55.9	32.7	31	28	54.8	59.6	55	58.6	14.5	37	16	18.2	12.4	15.4	34.9	18.8
Sm	10 <sup>-6</sup>	9.11	7.61	7.34	4.02	9.3	9.66	9.32	9.35	2.78	6.33	4.12	5.12	3.28	3.87	6.39	4.11
Eu	10 <sup>-6</sup>	1.84	0.84	0.83	0.87	0.98	0.97	1	1.02	0.88	0.97	0.21	0.16	0.16	0.18	0.95	0.59
Gd	10 <sup>-6</sup>	6.87	8.17	9.08	2.69	7.07	7.26	7.04	7.12	2.72	5.3	4.82	5.81	3.68	4.58	5.9	4.26
Tb	10 <sup>-6</sup>	0.94	1.51	1.79	0.4	1	0.98	0.93	0.91	0.43	0.79	0.98	0.99	0.71	0.87	0.95	0.77
Dy	10 <sup>-6</sup>	4.78	9.96	12.45	2.01	5.28	4.98	4.87	4.72	2.89	4.93	7.15	6.46	5.12	6.01	5.82	4.87
Ho	10 <sup>-6</sup>	0.8	2.25	2.89	0.36	0.95	0.83	0.84	0.84	0.62	0.98	1.61	1.41	1.12	1.34	1.18	1.01
Er	10 <sup>-6</sup>	1.85	6.75	8.57	0.91	2.53	2.14	2.34	2.17	1.97	2.97	5.13	4.34	3.74	4.38	3.67	3.05
Tm	10 <sup>-6</sup>	0.23	0.99	1.27	0.13	0.37	0.3	0.34	0.3	0.3	0.44	0.79	0.66	0.58	0.67	0.49	0.47
Yb	10 <sup>-6</sup>	1.33	5.69	7.56	0.8	2.32	1.9	2.27	2.08	2.13	2.97	5.72	4.86	4.37	4.89	3.52	3.28
Lu	10 <sup>-6</sup>	0.19	0.86	1.09	0.12	0.35	0.28	0.34	0.29	0.33	0.45	0.9	0.77	0.68	0.77	0.52	0.5
T <sub>w</sub>	℃	825.8	823.1	816.9	816.5	846.6	852.6	856.1	853.2	796.3	821.9	746.0	710.5	734.6	739.8	803.4	763.8

注: T<sub>w</sub>为岩浆结晶温度, 根据 Zr 在全岩中温度计方法计算(Watson et al., 1983)。

## 4.2 中天山、伊犁及塔里木地块新元古代早期(1.0~0.8 Ga)岩浆岩形成于后造山环境

通过对中天山、伊犁及塔里木地块新元古代早期岩浆岩(1.0~0.8 Ga)的野外考察、岩性、矿物组合、及全岩化学数据分析, 综合区域上已报道的同期花岗岩相关数据, 我们认为这些花岗岩并非形成在典型的大陆边缘弧环境。现今全球最典型的大陆边缘弧如南美安第斯弧、北美西海岸岩基(Sierra Nevada batholith、White-Inyo batholith、Peninsular Ranges batholith)以及藏南冈底斯岩石组合都以辉长岩、闪长岩和花岗闪长岩为主, 产状为大型岩基或岩体群, 矿物组合以富集角闪石为主要特征, 并常见大量基性包体(Qiu Jiansheng et al., 2015; Ma Xuxuan et al., 2017), 单矿物和全岩同位素都相对亏损, 具有显著的幔源物质贡献(Ardill et al., 2018; Ji Weiqiang et al., 2009; Ma Xuxuan et al.,

2018; Mo Xuanxue et al., 2005; Paterson et al., 2015; Saleeby et al., 2003; Ducea et al., 2007)。而中天山、伊犁及塔里木地块1.09~0.8 Ga的岩浆岩有如下特点: ①主要为花岗岩体, 全岩 SiO<sub>2</sub>重量百分比介于65%~80%之间(图 6a), 极少为闪长岩或花岗闪长岩; ②所有岩体规模都比较小, 多数为小岩体或岩株, 基本无大型岩基; ③岩体中未见早期基性包体; ④矿物组合中未见角闪石, 表明岩浆源区不富水, 与典型的俯冲相关弧型岩浆特征不符; ⑤单矿物和全岩同位素都较富集(Wang Zhongmei et al., 2014; Gao Jun et al., 2015; Huang Zongying et al., 2015a, b, 2017); ⑥含有大量捕获老锆石, 表明古老基底或重熔地壳的显著参与; ⑦高钾钙碱性和过铝质特征(图 6b 和 c); ⑧岩石源区主要为重熔基性下地壳(图 7a 和 b); ⑨构造背景判别图上基本落在后造山环境(图 8c 和 d)。这些特征说明中天

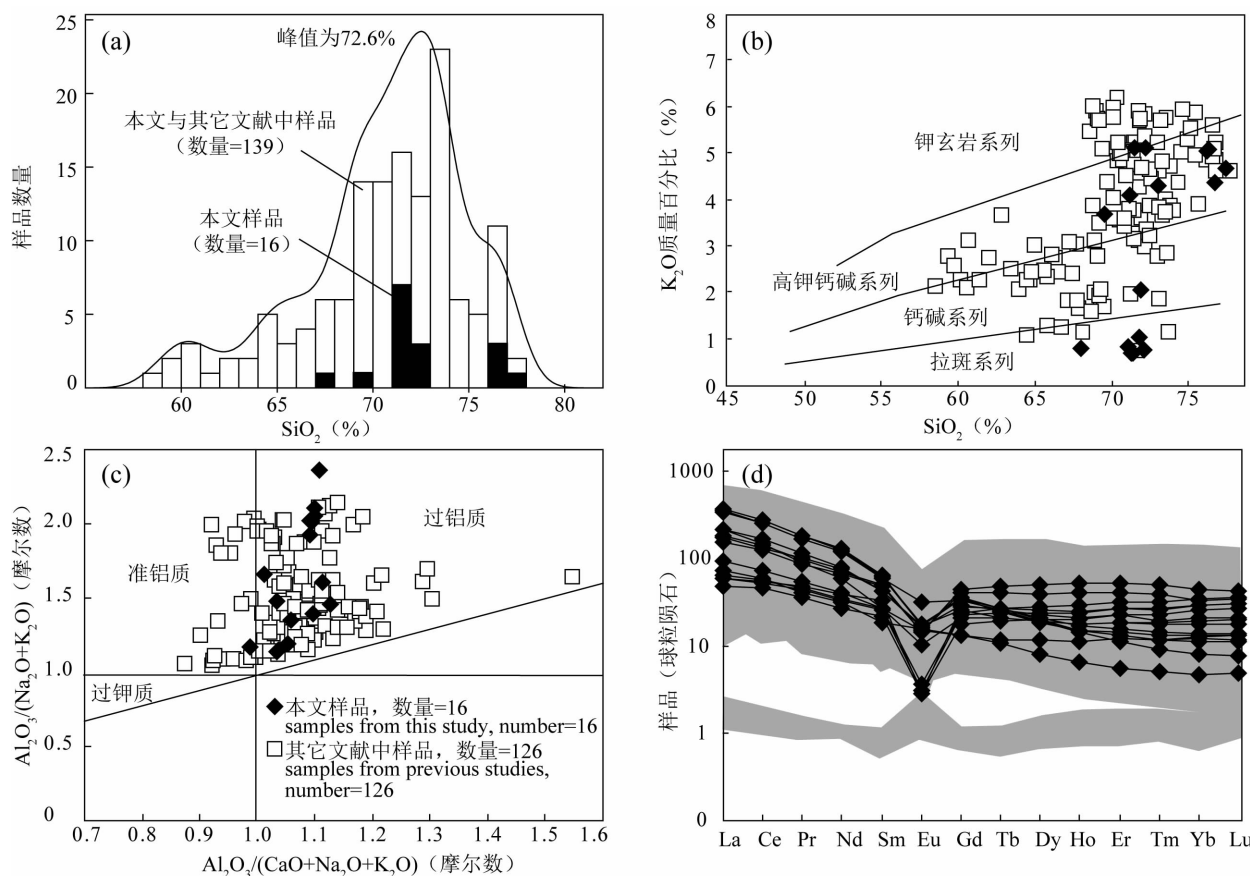


图 6 中天山、伊犁与塔里木地块新元古代早期花岗岩地球化学图解

Fig. 6 Geochemical diagrams for the Early Neoproterozoic granites in the present study and the reported ones in the Chinese Tianshan, Yili and Tarim blocks

(a)— $\text{SiO}_2$ 百分含量频率直方图;(b)— $\text{K}_2\text{O}$ - $\text{SiO}_2$ 图(Calanchi et al., 2002);(c)— $\text{Al}_2\text{O}_3/(\text{CaO}+\text{Na}_2\text{O}+\text{K}_2\text{O})-\text{Al}_2\text{O}_3/(\text{Na}_2\text{O}+\text{K}_2\text{O})$ 图(Maniar et al., 1989);(d)—REE球粒陨石标准化配分图(球粒陨石数据根据Sun S S et al., 1989)。数据来源(本文; Hu Aiqin et al., 2010; Li Ting et al., 2015; Wang Bo et al., 2014b; Gao Jun et al., 2015; Huang Botao et al., 2015; Huang Zongying et al., 2015, 2017; Zhang Chuanlin et al., 2007; Long Xiaoping et al., 2011; Wang Zhongmei et al., 2014; Wu Guanghui et al., 2018)

(a)—Relative probability of  $\text{SiO}_2$  contents; (b)— $\text{K}_2\text{O}$  vs.  $\text{SiO}_2$  diagram (after Calanchi et al., 2002); (c)—Diagram of  $\text{Al}_2\text{O}_3/(\text{CaO}+\text{Na}_2\text{O}+\text{K}_2\text{O})-\text{Al}_2\text{O}_3/(\text{Na}_2\text{O}+\text{K}_2\text{O})$  (after Maniar et al., 1989); (d)—Chondrite-normalized rare earth element (REE) patterns (The chondrite values are from Sun S S et al., 1989). Data sources are from this study, Hu Aiqin et al., 2010; Li Ting et al., 2015; Wang Bo et al., 2014b; Gao Jun et al., 2015; Huang Botao et al., 2015; Huang Zongying et al., 2015, 2017; Zhang Chuanlin et al., 2007; Long Xiaoping et al., 2011; Wang Zhongmei et al., 2014; Wu Guanghui et al., 2018)

山、伊犁及塔里木地块在新元古代早期已经进入后造山阶段,而非活动大陆边缘弧环境,即这些花岗岩既不是形成于罗迪尼亞超大陸初始汇聚的洋-陸俯冲阶段,也非罗迪尼亞超大陸形成后超大陸边缘洋-陸俯冲阶段。

#### 4.3 新元古代中天山、伊犁及塔里木地块的后造山高温岩浆成因

我们利用 Zr 在全岩中饱和温度计(Zr-in-whole rock)(Watson et al., 1983)和 Ti 在锆石中温度计(Ti-in-zircon)(Ferry et al., 2007; Watson et al., 2006)方法计算了中天山、伊犁及塔里木地块新元古

代早期岩体的结晶温度。结果显示岩体结晶温度普遍在 750~850 °C(图 8, 表 1)。说明本文岩体样品结晶温度较高。另外,我们利用 Zr 在全岩中饱和温度计算方法(Watson et al., 1983)计算了中天山、伊犁及塔里木地块已发表文献中共 126 件 1~0.8 Ga 岩浆岩样品的结晶温度,发现这些岩体的结晶温度也都比较高,普遍在 800 °C附近(图 8)。在后造山环境,形成高温岩浆的热源从何而来?我们认为这些热源很可能来自热毯效应(thermal blanket effect)(Trubitsyn et al., 2003; Braun, 2009; Yoshida et al., 2011)。大量陆块聚合成超大陆后,

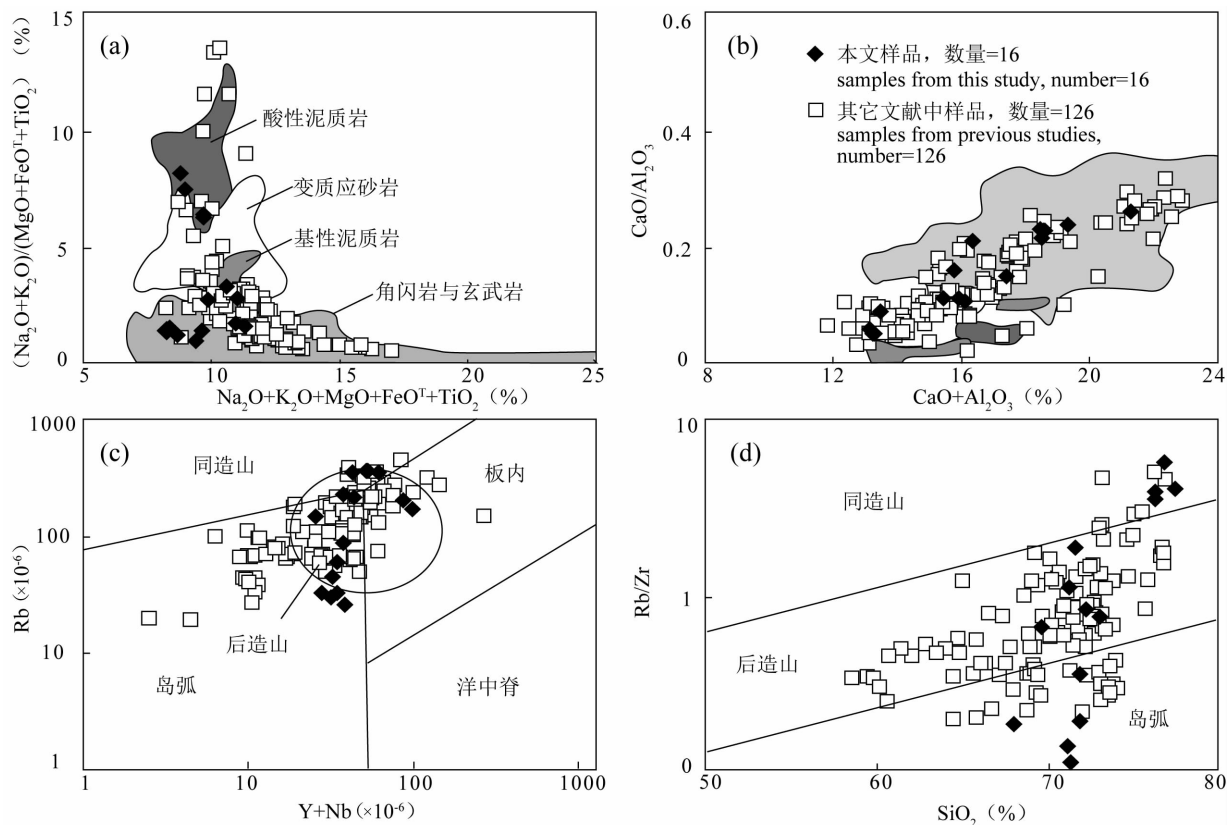


图 7 新元古代早期花岗岩(a)和(b)—源区判别图(修改自 Seo et al., 2010);(c)— $\text{Rb}/(\text{Y} + \text{Nb})$ 构造环境判别图(根据 Pearce, 1996);(d)— $\text{Rb}/\text{Zr}-\text{SiO}_2$ 构造环境判别图(根据 Harris et al., 1986);数据来源(本文; Hu Aiqin et al., 2010; Li Ting et al., 2015; Wang Bo et al., 2014b; Gao Jun et al., 2015; Huang Botao et al., 2015; Huang Zongying et al., 2015, 2017; Zhang Chuanlin et al., 2007; Long Xiaoping et al., 2011; Wang Zhongmei et al., 2014; Wu Guanghui et al., 2018.)  
 Fig. 7 (a) and (b) — Discriminate diagrams (after Seo et al., 2010); (c) —  $\text{Rb}/(\text{Y} + \text{Nb})$  tectonic setting diagram (after Pearce, 1996); (d) —  $\text{Rb}/\text{Zr}-\text{SiO}_2$  tectonic setting diagram for the early Neoproterozoic granites (after Harris et al., 1986). Data sources are from this study, Hu Aiqin et al., 2010; Li Ting et al., 2015; Wang Bo et al., 2014b; Gao Jun et al., 2015; Huang Botao et al., 2015; Huang Zongying et al., 2015, 2017; Zhang Chuanlin et al., 2007; Long Xiaoping et al., 2011; Wang Zhongmei et al., 2014; Wu Guanghui et al., 2018.)

由于超大陆热传导较慢、就像热毯一样,同时诱发巨量放辐射性热,这些热作用于岩石圈地幔或下地壳,从而促使岩石圈地幔或下地壳的部分熔融,进而形成较高温度的后造山花岗岩(Trubitsyn et al., 2003)。热毯效应形成的热异常是否是形成超级地幔柱的诱因,还有待更多的研究(Condie, 2004)。

#### 4.4 新元古代早期原塔里木陆块参与罗迪尼亞超大陆汇聚过程

最新的古地磁证据显示原塔里木盆地在 890~870 Ma 时已经位于罗迪尼亞超大陆内部(Wen Bin et al., 2017, 2018)(图 9),说明原塔里木盆地中的微陆块在 890~870 Ma 之前就已经开始了罗迪尼亞超大陆聚合过程(Wen Bin et al., 2018),即此时原塔里木盆地已经结束了洋陆俯冲过程、进入陆-陆碰撞或后碰撞造山阶段。这与全球其他陆块所记录

的 1.3~1.0 Ga 格林威尔造山(McLlland et al., 1996; Rogers, 1996)同期。虽然中天山、伊犁及塔里木盆地中的新元古代变形和岩浆不是原塔里木盆地参与罗迪尼亞超大陆最初洋-陆俯冲聚合过程的直接记录,但根据全球陆块参与罗迪尼亞超大陆汇聚过程特征,我们认为原塔里木盆地在 1.0~0.8 Ga 时曾与其他位置陆块碰撞,由于后期复杂的罗迪尼亞超大陆裂解及中亚造山带造山等过程,使得曾与原塔里木盆地相邻的未知陆块漂移到其他位置,二者之间的古老缝合带也随之漂移到其他位置或在后期造山过程中已剥蚀殆尽。另外,根据塔里木盆地中央位置(塔参 1 井)存在 1.2~1.0 Ga、具有岛弧特征的闪长岩-花岗闪长岩浆组合(李曰俊等,2003),推测塔里木盆地中央可能存在另外一条被第四系沉积物所掩盖的中-新元古代缝合带,此缝合带

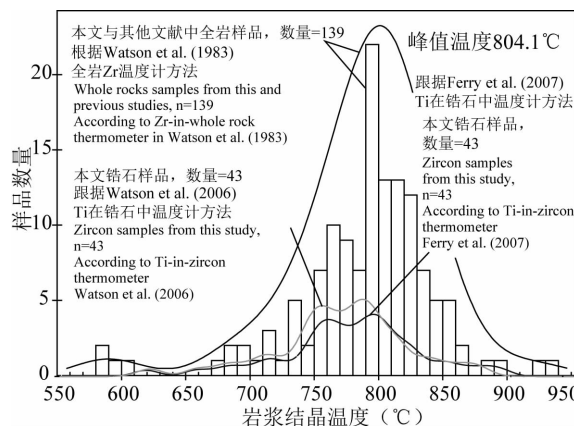


图 8 中天山、伊犁及塔里木地块新元古代早期花岗岩岩浆结晶温度频率统计图; Ti 在锆石温度计根据 Ferry et al. (2007) 与 Watson et al. (2006); 全岩 Zr 温度计根据 Watson et al. (1983); 数据来源(本文; Hu Aiqin et al., 2010; Li Ting et al., 2015; Wang Bo et al., 2014b; Gao Jun et al., 2015; Huang Botao et al., 2015; Huang Zongying et al., 2015, 2017; Zhang Chuanlin et al., 2007; Long Xiaoping et al., 2011; Wang Zhongmei et al., 2014; Wu Guanghui et al., 2018.)。

Fig. 8 Crystallization temperatures of the Early Neoproterozoic granites in the ChineseCentral Tianshan, Yili and Tarim blocks. Ti-in-zircon geothermometer after Ferry et al. (2007) and Watson et al. (2006). Zr-in-whole rock geothermometer after Watson et al. (1983). Data sources are from this study, Hu Aiqin et al., 2010; Li Ting et al., 2015; Wang Bo et al., 2014b; Gao Jun et al., 2015; Huang Botao et al., 2015; Huang Zongying et al., 2015, 2017; Zhang Chuanlin et al., 2007; Long Xiaoping et al., 2011; Wang Zhongmei et al., 2014; Wu Guanghui et al., 2018

代表罗迪尼亞超大陸形成後保留在南、北塔里木陸塊之間的殘余洋殼(如 Guo Zhaojie et al., 2005; Zhang Chuanlin et al., 2012; Xu Zhiqin et al., 2013)。

我们根据已有地质资料初步提出新元古代早期原塔里木陆块参与罗迪尼亞超大陆汇聚过程:

①>1.0 Ga 时, 原塔里木陆块向 N(现今方向)与某未知陆块汇聚, 同时在南原塔里木陆块和北原塔里木陆块之间发生洋-陆俯冲过程, 形成塔里木盆地塔参 1 井具有弧特征的闪长岩和花岗闪长岩(Li Yuejun et al., 2003)。而原塔里木陆块北缘此时可能处于被动大陆边缘环境, 没有典型的弧岩浆作用, 类似于中生代以来的印度大陆(Domeier et al., 2014; Kröner et al., 2016; Stampfli et al., 2002; Torsvik et al., 2012; Veevers, 2004; Xiao

Wenjiao et al., 2015)。此时原塔里木陆块已经开始向其它陆块汇聚, 为形成罗迪尼亞超大陆做贡献。

②1.0~0.8 Ga, 继上述洋-陆俯冲过程之后, 南原塔里木陆块和北塔里木陆块发生碰撞并拼合为统一陆块, 同时原塔里木陆块北缘与某未知陆块碰撞。此时原塔里木陆块已位于罗迪尼亞超大陆内部, 罗迪尼亞超大陆基本形成(图 9)。在原塔里木陆块北缘(中天山、伊犁及塔里木地块北缘)发生地壳部分熔融作用。类似于印度-亚洲大陆碰撞后, 印度北缘(现今的高喜马拉雅、低喜马拉雅)经历了显著的地壳深融及大量花岗岩侵位过程(Gao Li-E et al., 2016)。由于刚形成的罗迪尼亞超大陆的热毯效应造成中天山、伊犁及塔里木地块北缘的后造山岩浆岩的结晶温度偏高。又因为原塔里木陆块与某未知陆块碰撞后可能发生陆内斜向汇聚过程(类似于印度大陆斜向汇聚于亚洲大陆, Tapponier et al., 2001)从而促使原塔里木陆块北缘走滑剪切运动(图 9)。

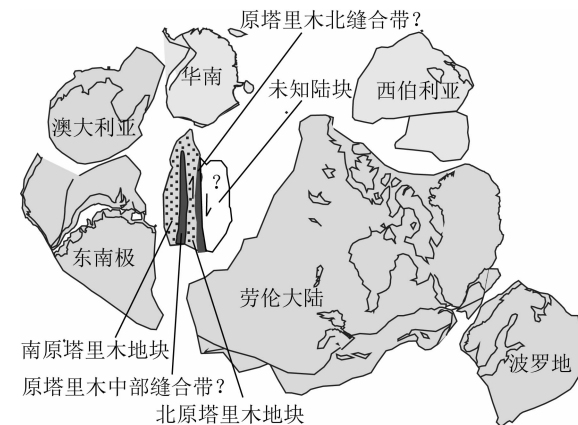


图 9 罗迪尼亞超大陸重建圖

(据 Wen Bin et al., 2018 修改)

Fig. 9 Reconstruction of Rodinia  
(modified after Wen Bin et al., 2018)

## 5 结论

本文系统分析和总结了中天山、伊犁及塔里木地块北缘新元古代早期(1.0~0.8 Ga)的构造变形及岩浆岩成分特征, 计算了岩体结晶温度。揭示了中天山、伊犁及塔里木地块新元古代早期的构造岩浆活动主要发生在后造山环境, 而非大陆边缘弧环境。综合区域地质资料, 说明原塔里木陆块北缘在新元古代早期已经位于超大陆的内部、完了成洋-陆汇聚阶段, 而其经历的陆-陆碰撞造山过程时间应为

>1.0 Ga, 可能与全球主要陆块一样, 发生在 1.3~1.0 Ga 格林威尔造山期。所以, 在罗迪尼亞超大陸聚合過程中, 中天山、伊犁及现今塔里木地塊最初参与罗迪尼亞超大陸汇聚阶段的时间应早于新元古代。

这一研究进展将为我们提供一个独特的视角去理解中国西北部三个主要陆块中天山、伊犁及塔里木地塊新元古早期演化历史, 并初步提出其参与罗迪尼亞超大陸汇聚过程, 进而引起我们对中国主要陆块比世界其他陆块开始参与罗迪尼亞超大陸聚合时间较晚问题的重新思考: 中国主要陆块记录的新元古代构造热事件可能只反映了罗迪尼亞超大陸晚期聚合过程, 而非初始阶段。若获得更成熟结论还需进行更多后续研究工作。

**致谢:**中国地质科学院地质研究所尹纪元、黄河及陈希节对初稿进行了评论, 并提出诸多后续性工作方向和建议, 在此一并感谢。

## References

- Anderson H E, Davis D W. 1995. U-Pb geochronology of the Moyie sills, Purcell Supergroup, southeastern British Columbia: implications for the Mesoproterozoic geological history of the Purcell (Belt) basin. Canadian journal of earth sciences, 32: 1180~1193.
- Ardill K, Paterson S, Memeti V. 2018. Spatiotemporal magmatic focusing in upper-mid crustal plutons of the Sierra Nevada arc. Earth and Planetary Science Letters, 498: 88~100.
- Berry R F, Holm, O H, Steele D A. 2005. Chemical U-Th-Pb monazite dating and the Proterozoic history of King Island, southeast Australia. Australian journal of earth sciences, 52: 461~471.
- Bogdanova S V, Pisarevsky S A, Li Zhengxiang. 2009. Assembly and breakup of Rodinia (Some results of IGCP project 440). Stratigraphy and Geological Correlation, 17: 29~45.
- Braun J. 2009. Hot blanket in Earth's deep crust. Nature, 458: 292~293.
- Bruguier O, Bosch D, Pidgeon R T, Byrne D I, Harris L B. 1999. U-Pb chronology of the Northampton Complex, Western Australia: evidence for Grenvillian sedimentation, metamorphism and deformation and geodynamic implications. Contributions to mineralogy and petrology, 136: 258~272.
- Calanchi N, Peccerillo A, Tranne C A, Lucchini F, Rossi P L, Kempton P, Barbieri, M, Wu T W. 2002. Petrology and geochemistry of volcanic rocks from the island of Panarea: implication for mantle evolution beneath the Aeolian island arc (southern Tyrrhenian sea). Journal of Volcanology and Geothermal Research, 115: 367~395.
- Charvet J, Shu Liangshu, Laurent-Charvet S, Wang Bo, Faure M, Cluzel D, Chen Yan, Jong K D. 2011. Palaeozoic tectonic evolution of the Tianshan belt, NW China. Science China Earth Sciences, 54: 166~184.
- Charvet J, Shu Liangshu, Laurent-Charvet S. 2007. Paleozoic structural and geodynamic evolution of eastern Tianshan (NW China): welding of the Tarim and Junggar plates. Episodes, 30: 162~186.
- Chen Xijie, Shu Liangshu, Santosh M, Zhao Xixi. 2013. Island arc-type bimodal magmatism in the eastern Tianshan Belt, Northwest China: Geochemistry, zircon U-Pb geochronology and implications for the Paleozoic crustal evolution in Central Asia. Lithos, 168~169: 48~66.
- Chen Xinyue, Wang Yuejun, Sun Linhua, Fan Weiming. 2009. Zircon SHRIMP U-Pb dating of the granitic gneisses from Bingdaban and Laerdundaban (TianshanOrogen) and their geological Significances. Geochimica, 38: 424~431 (in Chinese with English abstract).
- Chen Yibing, Hu Aiqin, Zhang Guoxin, Zhang Qianfeng. 1999. Zircon U-Pb age and Nd-Sr isotopic composition of granitic gneiss and its geological implications from Precambrian window of western Tianshan, NW China. Geochimica, 28(6): 515~520 (in Chinese with English abstract).
- Chen Yibing, Hu Aiqin, Zhang Guoxin, Zhang Qianfeng. 2000. Precambrian basement age and characteristics of Southwestern Tianshan: zircon U-Pb geochronology and Nd-Sr isotopic compositions. Acta Petrologica Sinica, 16(1): 91~98 (in Chinese with English abstract).
- Condie K C. 1998. Episodic continental growth and supercontinents: a mantle avalanche connection? Earth and Planetary Science Letters, 163: 97~108.
- Condie K C. 2004. Supercontinents and superplume events: distinguishing signals in the geological record. Physics of the Earth and Planetary Interiors, 146: 319~332.
- Deng Xingliang, Shu Liangshu, Zhu Wenbin, Ma Dongsheng, Wang Bo. 2008. Precambrian tectonism, magmatism, deformation and geochronology of igneous rocks in the Xingdi fault zone, Xinjiang. Acta petrologica Sinica, 24(12): 2800~2808 (in Chinese with English abstract).
- Domeier M, Torsvik T H. 2014. Plate tectonics in the late Paleozoic. Geoscience Frontiers, 5: 303~350.
- Dong Yunpeng, Zhang Guowei, Neubauer F, Liu Xiaoming, Hauzenberger C, Zhou Dingwu, Li Wei. 2011. Syn-and post-collisional granitoids in the Central Tianshan orogen: Geochemistry, geochronology and implications for tectonic evolution. Gondwana Research, 20: 568~581.
- Ducea M N, Barton M D. 2007. Igniting flare-up events in Cordilleran arcs. Geology, 35(11): 1047~1050.
- Evans D A D. 2013. Reconstructing pre-Pangean supercontinents. GSA Bulletin, 125: 11~12.
- Ferry J M, Watson E B. 2007. New thermodynamic models and revised calibrations for the Ti-in-zircon and Zr-in-rutile thermometers: Contributions to Mineralogy and Petrology, 154: 429~437.
- Gao Jun, Wang Xinshui, Klemd R, Jiang Tuo, Qian Qing, Mu Lixiu, Ma Yuzhou. 2015. Record of assembly and breakup of Rodinia in the Southwestern Altaiids: Evidence from Neoproterozoic magmatism in the Chinese Western TianshanOrogen. Journal of Asian Earth Sciences, 113: 173~193.
- Gao Li-E, Zeng Lingsen, Asimow P D. 2016. Contrasting geochemical signatures of fluid-absent versus fluid-fluxed melting of muscovite in metasedimentary sources: The Himalayan leucogranites. Geology, doi: 10.1130/G38336.1.
- Ge Rongfeng, Zhu Wenbin, Wilde S A, He Jingwen, Cui Xiang. 2015. Synchronous crustal growth and reworking recorded in late Paleoproterozoic granitoids in the northern Tarim craton: In situ zircon U-Pb-Hf-O isotopic and geochemical constraints and tectonic implications. GSA Bulletin, 127: 781~803.
- Ge Rongfeng, Zhu Wenbin, Wilde S A. 2016. Mid-Neoproterozoic (ca. 830~800 Ma) metamorphic P-T paths link Tarim to the circum-Rodinia subduction-accretion system. Tectonics, 35: 1465~1488.
- Ge Rongfeng, Zhu Wenbin, Wu Hailin, Zheng Bihai, He Jingwen. 2013. Timing and mechanisms of multiple episodes of migmatization in the Korla Complex, northern Tarim Craton, NW China: Constraints from zircon U-Pb-Lu-Hf isotopes and implications for crustal growth. Precambrian Research, 231: 136~156.

- Ge Rongfeng, Zhu Wenbin, Wu Hailin, Zheng Bihai, Zhu Xiaoqing, He Jinwen. 2012. The Paleozoic northern margin of the Tarim Craton: Passive or active? *Lithos*, 142~143: 1~15.
- Gose W A, Helper M A, Connelly J N, Hutson F E, Dalziel I W D. 1997. Paleomagnetic data and U-Pb isotopic age determinations from Coats Land Antarctica; implications for late Proterozoic plate reconstructions. *Journal of Geophysical Research. B*, 102: 7887~7902.
- Guo Zhaojie, Yin An, Robinson A, Jia Chengzao. 2005. Geochronology and geochemistry of deep-drill-core samples from the basement of the central Tarim basin. *Journal of Asian Earth Sciences*, 25: 45~56.
- Han Baofu, He Guoqi, Wang Xuechao, Guo Zhaojie. 2011. Late Carboniferous collision between the Tarim and Kazakhstan-Yili terranes in the western segment of the South Tian Shan Orogen, Central Asia, and implications for the Northern Xinjiang, western China. *Earth Science Reviews*, 109: 74~93.
- Harris N B W, Pearce J A, Tindle A G. 1986. Geochemical characteristics of collision-zone magmatism. In: Caward, M. P., Reis, A. S. (Eds.), *CollisionTectonics*; Geological Society of London, Special Publication, 19: 67~81.
- He Zhenyu, Zhang Zeming, Zong Keqing, Dong Xin. 2013. Paleoproterozoic crustal evolution of the tarim craton: constrained by zircon U-Pb and Hf isotopes of meta-igneous rocks from Korla and Dunhuang. *Journal of Asian Earth Sciences*, 78(12): 54~70.
- Hoffman P F, Kaufman A J, Halverson G P, Schrag D P. 1998. A Neoproterozoic snowball earth. *Science*, 281: 1342~1346.
- Hoffman P F. 1992. Supercontinents. *Encyclopedia of Earth Systems Science*, vol. 4. Academic Press, London, pp. 323~328.
- Hu Aiqin, Jahn Borming, Zhang Guoxin, Chen Yibing, Zhang Qianfeng. 2000. Crustal evolution and Phanerozoic crustal growth in northern Xinjiang: Nd isotopic evidence. Part I: Isotopic characterization of basement rocks. *Tectonophysics*, 328: 15~51.
- Hu Aiqin, Wei Gangjian, Jahn Borming, Zhang Jibin, Deng Wenfeng, Chen Linli. 2010. Formation of the 0. 9 Ga Neoproterozoic granitoids in the Tianshan Orogen, NW China: constraints from the SHRIMP zircon age determination and its tectonic significance. *Geochimica*, 39 (3): 197~212 (in Chinese with English abstract).
- Hu Zhaochu, Zhang Wen, Liu Yongsheng, Gao Shan, Li Ming, Zong Keqing, Chen Haihong, Hu Shenghong. 2015. "Wave" signal smoothing and mercury removing device for laser ablation quadrupole and multiple collector ICP-MS analysis: application to lead isotope analysis. *Analytical Chemistry*, 87: 1152~1157.
- Hu, Aiqin, Wei Gangjian. 2006. On the age of the Neo-Archean Qingir Gray Gneisses from the Northern Tarim Basin, Xinjiang, China. *Acta Geological Sinica* 80, 126~134 (in Chinese with English Abstract).
- Huang Botao, He Zhenyu, Zhang Zeming, Klemd R, Zong Keqing, Zhao Zhidan. 2015. Early Neoproterozoic granitic gneisses in the Chinese Eastern Tianshan: petrogenesis and tectonic implications. *Journal of Asian Earth Sciences*, 113: 339~352.
- Huang He, Zhang Zhaochong, Santosh M, Cheng Zhiguo, Wang Tao. 2019. Crustal evolution in the South Tianshan Terrane; constraints from detrital zircon geochronology and implications for continental growth in the Central Asian Orogenic Belt. *Geological Journal*, 54: 1379~1400.
- Huang Hu, Cawood, P A, Hou Mingcai, Xiong Fuhalo, Ni Shijun, Gong Tingting. 2019. Provenance of latest Mesoproterozoic to early Neoproterozoic (meta)-sedimentary rocks and implications for paleogeographic reconstruction of the Yili Block. *Gondwana Research*, 72: 120~138.
- Huang Zongying, Long Xiaoping, Kroner A, Yuan Chao, Wang Yujing, Chen Bei, Zhang Yunying. 2015. Neoproterozoic granitic gneisses in the Chinese Central Tianshan Block: implications for tectonic affinity and Precambrian crustal evolution. *Precambrian Research*, 269: 73~89.
- Huang Zongying, Long Xiaoping, Wang Xuance, Zhang Yunyi. Du Long, Yuan Chao, Xiao Wenjiao. 2017. Precambrian evolution of the Chinese Central Tianshan Block: constraints on its tectonic affinity to the Tarim Craton and response to supercontinental cycles. *Precambrian Research*, 295: 24~37.
- Jacobs J, Bauer W, Fanning C M. 2003. New age constraints for Grenville-age metamorphism in western central Dronning Maud Land (East Antarctica), and implications for the palaeogeography of Kalahari in Rodinia. *International journal of Earth Sciences*, 92: 301~315.
- Jahn Borming. 2004. The Central Asia Orogenic Belt and growth of the continental crust in the Phanerozoic. In: Malpas, J, Fletcher, C. J. N, Ali, J. R, Aitchison, J. C. (Eds.), *Aspects of the Tectonic Evolution of China*. Geological Society, Special Publications, 226, London, pp. 73~100.
- Ji Weiqiang, Wu Fuyuan, Chung Sunlin, Li Jinxiang, Liu Chuanzhou. 2009. Zircon U-Pb geochronology and Hf isotopic constraints on petrogenesis of the Gangdese batholith, southern Tibet. *Chemical Geology*, 262: 229~245.
- Kirschvink J L. 1992. Late Proterozoic low-latitude glaciation: the snowball Earth. In: Schopf J W, Klein C. (Eds.), *The Proterozoic Biosphere: A Multidisciplinary Study*. Cambridge University Press, Cambridge, UK, pp. 51~52.
- Kr?ner A, Windley B F, Badarch G, Tomurtogoo O, Hegner E, Jahn Borming, Gruschka S, Khain E V, Demoux A, Wingate M T D. 2007. Accretionary growth and crust-formation in the Central Asian Orogenic Belt and comparison with the Arabian-Nubian shield. *Geological Society of America Memoirs*, 200: 181~209.
- Kr?ner U, Roscher M, Romer R L. 2016. Ancient plate kinematics derived from the deformation pattern of continental crust: Paleo-and Neo-Tethys opening coeval with prolonged Gondwana-Laurussia convergence. *Tectonophysics*, 681: 220~233.
- Lei Ruxiong, Wu Changzhi, Chi Guoxiang, Gu Lianxing, Dong Lianhui, Qu Xun, Jiang Yaohui, Jiang Shaoyong. 2013. The Neoproterozoic Hongliujing A-type granite in Central Tianshan (NW China): LA-ICP-MS zircon U-Pb geochronology, geochemistry, Nd-Hf isotope and tectonic significance. *Journal of Asian Earth Sciences*, 74: 142~154.
- Li Qiugen, Liu Shuwen, Han Baofu, Zhang Jian, Chu Zhuyin. 2003. Nd isotopic characteristics of Proterozoic metasedimentary rocks and constraints on their provenance in the eastern segment of Central Tianshan Belt, Xinjiang. *Progress in Nature Science*, 13: 908~913.
- Li Ting, Li Zhipei, BaiJianke, Li Xiaoying. 2015. Geochronology, Geochemistry of Dagenbieli Neoproterozoic granites in the Yili block, and its geological implications. *Northwestern Geology*, 48 (3): 96~111 (in Chinese with English abstract).
- Li Yuejun, Sun Longde, Hu Shiling, Song Wenjie, Wang Guolin, Tan Zejin. 2003.  $^{40}\text{Ar}$ - $^{39}\text{Ar}$  geochronology of the granite and diorite revealed at the bottom of Tacan 1, the deepest well in China. *Acta Petrologica Sinica*, 19 (3): 530~536 (in Chinese with English abstract).
- Li Z X, Bogdanova S V, Collins A S, Davidson A, De Waele B, Ernst R E, Fitzsimons I C W, Fuck R A, Gladkochub D P, Jacobs J, Karlstrom K E, Lu S, Natapov L M, Pease V, Pisarevsky S A, Thrane K, Vernikovsky V. 2008. Assembly, configuration, and break-up history of Rodinia: a synthesis. *Precambrian Research* 160: 179~210.
- Li Zhengxiang, Li Xianhua, Zhou Hanwen, Kinny P D. 2002. Grenvillian continental collision in South China: new SHRIMP U-Pb zircon results and implications for the configuration of Rodinia. *Geology*, 30, 163~166.
- Li Zhengxiang, Zhang Linghua, Powell C M. 1995. South China in Rodinia: part of the missing link between Australia-East

- Antarctica and Laurentia? *Geology*, 23: 407~410.
- Liu Shuwen, Guo Zhaojie, Zhang Zhaochong, Li Qiugen, Zheng Haifei. 2004. Nature of the Precambrian metamorphic blocks in the eastern segment of Central Tianshan: constraint from geochronology and Nd isotopic geochemistry. *Science in China D*, 47 (12): 1085~1094.
- Liu Ying, Liu H C, Li X H. 1996. Simultaneous and precise determination of 40 trace elements in rock samples using ICP-MS. *Geochimica*, 25 (6): 552~558 (in Chinese with English abstract).
- Liu Yongsheng, Gao Shan, Hu Zhaochu, Gao Changgui, Zong Keqing, Wang Dongbing. 2010. Continental and oceanic crust recycling-induced melt-peridotite interactions in the Trans-North China Orogen: U-Pb dating, Hf isotopes and trace elements in zircons of mantle xenoliths. *Journal of Petrology*, 51: 537~571.
- Long Xiaoping, Yuan Chao, Sun Min, Kr? ner A, Zhao Guochun, Wilde S A, Hu Aiqin. 2011. Reworking of the Tarim Craton by underplating of mantle plume-derived magmas: evidence from Neoproterozoic adakitic rocks and I-type granites in the Kuluketage area, NW China. *Precambrian Research*, 187: 1~14.
- Long Xiaoping, Yuan Chao, Sun Min, Zhao Guochun, Xiao Wenjiao, Wang Yujing, Yang Yueheng, Hu Aiqin. 2010. Archean crustal evolution of the northern Tarim Craton, NW China: zircon U-Pb and Hf isotopic constraints. *Precambrian Research*, 187: 1~14.
- Lu Songnian, Li Huaikun, Zhang Chuanlin, Niu Guanghua. 2008. Geological and geochronological evidence for the Precambrian evolution of the Tarim Craton and surrounding continental fragments. *Precambrian Research*, 160: 94~107.
- Ludwig K R. 2003. ISOPLOT 3.00: A Geochronological Toolkit for Microsoft Excel. Berkeley Geochronology Center, California, Berkeley, 39 pp.
- Ma Xuxuan, Meert J G, Xu Zhiqin, Yi Zhiyu. 2018. Late Triassic intra-oceanic arc system within Neotethys: Evidence from cumulate appinite in the Gangdese belt, southern Tibet. *Lithosphere*, 10: 545~565.
- Ma Xuxuan, Meert J G, Xu Zhiqin, Zhao Zhongbao. 2017. Evidence of magma mixing identified in the Early Eocene Caina pluton from the Gangdese Batholith, southern Tibet. *Lithos*, 278~281: 126~139.
- Ma Xuxuan, Shu Liangshu, Meert J G, Li Jinyi. 2014a. The Paleozoic evolution of Central Tianshan: geochemical and geochronological evidence. *Gondwana Research*, 25: 797~819.
- Ma Xuxuan, Shu Liangshu, Meert J G, Xu Zhiqin. 2014b. The fingerprint of Precambrian basement in the Chinese Central Tianshan: evidence from inherited/xenocrystic zircons of magmatic rocks. *Geological Magazine*, 1~8.
- Ma Xuxuan, Shu Liangshu, Meert J G. 2015. Early Permian slab breakoff in the Chinese Tianshan belt inferred from the post-collisional granitoids. *Gondwana Research*, 27: 228~243.
- Ma Xuxuan, Shu Liangshu, Santosh M, Li Jinyi. 2012. Detrital zircon U-Pb geochronology and Hf isotope data from Central Tianshan suggesting a link with the Tarim Block: Implications on Proterozoic supercontinent history. *Precambrian Research*, 206~207: 1~16.
- Maniar P D, Piccoli P M. 1989. Tectonic discrimination of granitoids. *Geological Society of American Bulletin*, 101: 635~643.
- McLelland J, Daly J S, McLelland J M. 1996. The Grenville Orogenic Cycle (ca. 1350-1000 Ma): an Adiron-dack perspective. *Tectonophysics*, 265: 1~28.
- McMenamin M A S, McMenamin D L S. 1990. *The Emergence of Animals: The Cambrian Breakthrough*. Colombia University Press, New York, 217 pp.
- Meert J G. 2012. What's in a name? The Columbia (Paleopangaea/Nuna) supercontinent. *Gondwana Research*, 21: 987~993.
- Mo Xuanxue, Dong Guochen, Zhao Zhdan, Zhou Su, Wang Liangliang, Qiu Ruizhao, Zhang Fengqin. 2005. Spatial and temporal distribution and characteristics of granitoids in the Gangdese, Tibet and implication for crustal growth and evolution. *Geological Journal of China Universities*, v. 11, p. 281~290 (in Chinese with English abstract).
- Moores E M. 1991. Southwest U. S.-East Antarctic (SWEAT) connection: a hypothesis. *Geology*, 19: 425~428.
- Paterson S R, Ducea M N. 2015. Arc Magmatic Tempos: Gathering the Evidence; Elements, 11: 91~98.
- Pearce J A. 1996. Source and setting of granitic rocks. *Episodes*, 19: 120~125.
- Powell C M, Li Zhengxiang, McElhinny M W, Meert J G, Park J K. 1993. Paleomagnetic constraints on timing of the Neoproterozoic breakup of Rodinia and the Cambrian formation of Gondwana; with Suppl Data 9335. *Geology*, 21: 889~892.
- Powell C M, Pisarevsky S A. 2002. Late Neoproterozoic assembly of East Gondwana. *Geology*, 30: 3~6.
- Qiu Jiansheng, Wang Ruiqiang, Zhao Jiaolong, Yu Sibin. 2015. Petrogenesis of the Early Jurassic gabbro-granite complex in the middle segment of the Gangdese belt and its implications for tectonic evolution of Neo-Tethys: a case study of the Dongga pluton in Xigaze. *Acta Petrologica Sinica*, 31: 3569~3580 (in Chinese with English abstract).
- Rogers J J W, Santosh M. 2003. Supercontinents in Earth History. *Gondwana Research*, 6(3): 357~368.
- Rogers J J W, Santosh M. 2009. Tectonics and surface effects of the supercontinent Columbia. *Gondwana Research*, 15: 373~380.
- Rogers J J W. 1996. A history of continents in the past three billion years. *Journal of Geology*, 104: 91~107.
- Saleby J, Ducea M N, Clemens-Knott D. 2003. Production and loss of high-density batholithic root, southern Sierra Nevada, California. *Tectonics*, 22: 1064.
- Seo J, Choi S G, Oh C W. 2010. Petrology, Geochemistry, and geochronology of the post-collisional Triassic mangerite and syenite in the Gwangcheon area, Hongseong Belt, South Korea. *Gondwana Research*, 18: 479~496.
- Shu L S, Deng X L, Zhu W B, Ma D S, Xiao W J. 2011. Precambrian tectonic evolution of the Tarim Block, NW China: new geochronological insights from the Quruqtagh domain. *Journal of Asian Earth Sciences*, 42: 774~790.
- Shu Liangshu, Charvet J, Lu Huafu, Laurent S C. 2002. Paleozoic Accretion-Collision Events and Kinematics of Ductile Deformation in the Eastern Part of the Southern-Central Tianshan Belt, China. *Acta Geologica Sinica-English Edition*, 76: 308~323.
- Shu Liangshu, Charvet J, Ma Ruishi. 1998. Study of a large scale Paleozoic dextral strike-slip ductile shear zone along the northern margin of the Central Tianshan, Xinjiang. *Xinjiang Geology*, 16(4): 326~336 (in Chinese with English abstract).
- Shu Liangshu, Chen Yuntang, Lu Huafu, Charvet J, Laurent-Charvet S, Yin Donghao. 2000. Paleozoic Accretionary Terranes in Northern Tianshan, NW China. *Chinese Journal of Geochemistry-English Edition*, 19: 193~202.
- Shu Liangshu, Wang Bo, Zhu Wenbin, Guo Zhaojie, Charvet J, Zhang Yuan. 2011. Timing of initiation of extension in the Tianshan, based on structural, geochemical and geochronological analyses of bimodal volcanism and olistostrome in the Bogda Shan (NW China). *International Journal of Earth Sciences*, 100: 1647~1663.
- Stampfli G M, Borel G D. 2002. A plate tectonic model for the Paleozoic and Mesozoic constrained by dynamic plate boundaries and restored synthetic oceanic isochrons. *Earth and Planetary Science Letters*, 196: 17~33.
- Sun S S, McDonough W F. 1989. Chemical and isotopic systematics of oceanic basalts: implications for mantle composition and processes. *Geological Society, London, Special Publications*, 42: 313~345.
- Sun Xiaomeng, Wang Pujun, Liu Pengju, Hao Fujiang. 2006.

- Structural features and tectonic evolutionary history of Xingdi fault. *Xijiang Geology*, 24 (4): 348~352 (in Chinese with English abstract).
- Tapponier P, Xu Zhiqin, Roger F, Meyer Bertrand, Arnaud N, Wittlinger G, Yang Jingsui. 2001. Oblique stepwise rise and growth of the Tibet plateau. *Science*, 294: 671~678.
- Torsvik T H, Van der Voo R, Preeden U, Mac Niocaill C, Steinberger B, Doubrovine P V, van Hinsbergen D J J, Domeier M, Gaina C, Tohver E, Meert J G, McCausland, P J A, Cocks L R M. 2012. Phanerozoic polar wander, palaeogeography and dynamics. *Earth-Science Reviews*, 114: 325~368.
- Trubitsyn V P, Mooney W D, Abbott D H. 2003. Cold cratonic roots and thermal blankets: How continents affect mantle convection. *International Geology Review*, 45: 479~496.
- Veevers J J. 2004. Gondwanaland from 650~500 Ma assembly through 320 Ma merger in Pangea to 185~100 Ma breakup: supercontinental tectonics via stratigraphy and radiometric dating. *Earth-Science Reviews*, 68: 1~132.
- Wang Bo, Faure M, Shu Liangshu, Jong K D, Charvet J, Cluzel D, Jahn B M, Chen Yan, Ruffet G. 2010. Structural and Geochronological Study of High-Pressure Metamorphic Rocks in the Kekesu Section (Northwestern China): Implications for the Late Paleozoic Tectonics of the Southern Tianshan. *The Journal of Geology*, 118: 59~77.
- Wang Bo, Liu Hongsheng, Shu Liangshu, Jahn Borming, Chung Sunlin, Zhai Yazhong, Liu Dunyi. 2014b. Early Neoproterozoic crustal evolution in northern Yili Block: Insights from migmatite, orthogneiss and leucogranite of the Wenquan metamorphic complex in the NW Chinese Tianshan. *Precambrian Research*, 242(3): 58~81.
- Wang Bo, Shu Liangshu, Liu Hongsheng, Gong Hujun, Ma Yuzhou, Mu Lixiu, Zhong Linglin. 2014a. First evidence for ca. 780 Ma intra-plate magmatism and its implications for Neoproterozoic rifting of the North Yili Block and tectonic origin of the continental blocks in SW of Central Asia. *Precambrian Research*, 254: 258~272.
- Wang Chao, Wang Yonghe, Liu Liang, He Shiping, Li Rongshe, Li Meng, Yang Wenqiang, Cao Yuting, Meert J G, Shi Chao. 2014. The Paleoproterozoic magmatic-metamorphic events and cover sediments of the Tieliklik Belt and their tectonic implications for the southern margin of the Tarim Craton, northwestern China. *Precambrian Research*, 254: 210~225.
- Wang Chao, Zhang Jiheng, Li Meng, Li Rongshe, Peng Yan. 2015. Generation of ca. 900~870 Ma bimodal rifting volcanism along the southwestern margin of the Tarim Craton and its implications for the Tarim-North China connection in the early Neoproterozoic. *Journal of Asian Earth Sciences*, 113: 610~625.
- Wang Xinshui, Gao Jun, Klemd R, Jiang Tuo, Li Jilei, Zhang Xi, Xue Shengchao. 2017. The Central Tianshan Block: A microcontinent with a Neoarchean-Paleoproterozoic basement in the southwestern Central Asian Orogenic Belt. *Precambrian Research*, 295: 130~150.
- Wang Zhongmei, Han Chunming, Xiao Wenjiao, Su Benxun, Sakyi P A, Song Dongfang, Lin Lina. 2014. The petrogenesis and tectonic implications of the granitoid gneisses from Xingxingxia in the eastern segment of Central Tianshan. *Journal of Asian Earth Sciences*, 88: 277~292.
- Watson B E, Harrison M T. 1983. Zircon saturation revisited: temperature and composition effects in a variety of crustal magma types. *Earth and Planetary Science Letters*, 64: 295~304.
- Watson E B, Wark D A, Thomas J B. 2006. Crystallization thermometers for zircon and rutile: Contributions to Mineralogy and Petrology, 151: 413~433.
- Weil A B, Voo R V D, Niocaill C M, Meert J G. 1998. The Proterozoic supercontinent Rodinia: paleomagnetically derived reconstructions for 1100 to 800 Ma. *Earth and Planetary Science Letters*, 154(1~4): 0~24.
- Wen Bin, Evans D A D, Li Yongxiang. 2017. Neoproterozoic paleogeography of the Tarim Block: An extended or alternative "missing-link" model for Rodinia? *Earth and Planetary Science Letters*, 458: 92~106.
- Wen Bin, Evans D A D, Wang Chao, Li Yongxiang, Jing Xianqing. 2018. A positive test for the Greater Tarim Block at the heart of Rodinia: Mega-dextral suturing of supercontinent assembly. *Geology*, 46: 687~690.
- Windley B F, Alexeiev D, Xiao W J, Krone A, Badarch G. 2007. Tectonic models for accretion of the Central Asian Orogenic Belt. *Journal of the Geological Society*, 164: 31~47.
- Wu Guanghui, Xiao Yang, Bonin B, Ma Debo, Li Xin, Zhu Guangyou. 2018. Ca. 850 Ma magmatic events in the Tarim Craton: age, geochemistry and implications for assembly of Rodinia supercontinent. *Precambrian Research*, 305: 489~503.
- Wu Hailin, Zhu Wenbin, Ge Rongfeng. 2019. Late Paleoproterozoic granulite-facies metamorphism in the North Altyn Tagh area, southeastern Tarim craton: pressure-temperature paths, zircon U-Pb ages, and tectonic implications. *GSA Bulletin*, doi: 10.1130/B35085.1.
- Xiao Wenjiao, Huang Baochun, Han Chunming, Sun Shu, Li Jiliang. 2010. A review of the western part of the Altaids: a key to understanding the architecture of accretionary orogens. *Gondwana Research*, 18: 253~273.
- Xiao Wenjiao, Windley B F, Sun Shu, Li Jiliang, Huang Baochun, Han Chunming, Yuan Chao, Sun Min, Chen Hanlin. 2015. A Tale of Amalgamation of Three Permo-Triassic Collage Systems in Central Asia: Oroclines, Sutures, and Terminal Accretion. *Annual Review of Earth and Planetary Sciences*, 43: 477~507.
- Xiong Fuhan, Hou Mingcai, Cawood P A, Huang Hu, Ducea M N, Ni Shijun. 2019. Neoproterozoic I-type and highly fractionated A-type granites in the Yili Block, Central Asian Orogenic Belt: Petrogenesis and tectonic implications. *Precambrian Research*, 328: 235~249.
- Xu Bei, Jian Ping, Zheng Haifei, Zou Haibo, Zhang Lifei, Liu Dunyi. 2005. U-Pb zircon geochronology and geochemistry of Neoproterozoic volcanic rocks in the Tarim Block of northwest China: implications for the breakup of Rodinia supercontinent and Neoproterozoic glaciations. *Precambrian Research*, 136 (2): 107~123.
- Xu Zhiqin, He Bizhu, Zhang Chuanlin, Zhang Jianxin, Wang Zhaoming, Cai Zhihui. 2013. Tectonic framework and crustal evolution of the Precambrian basement of the Tarim Block in NW China: New geochronologic evidence from deep drilling samples. *Precambrian Research*, 235: 150~162.
- Yao Jinlong, Cawood P A, Shu Liangshu, Santosh M, Li Jinyi. 2016. An Early Neoproterozoic accretionary prism ophiolitic melange from the Western Jiangnan Orogenic Belt, South China. *The Journal of Geology*, 124: 587~601.
- Yin Jiyuan, Yuan Chao, Sun Min, Long Xiaoping, Zhao Guochun, Wong K P, Geng Hongyan, Cai Keda. 2010. Late Carboniferous high-Mg dioritic dikes in Western Junggar, NW China: Geochemical features, petrogenesis and tectonic implications. *Gondwana Research*, 17: 145~152.
- Yoshida M, Santosh M. 2011. Supercontinents, mantle dynamics and plate tectonics: A perspective based on conceptual vs. numerical models. *Earth-Science Reviews*, 105: 1~24.
- Yu Shengyao, Zhang Jianxin, Zhao Xilin, Gong Jianghua, Li Yunshuai. 2013. Geochronology, geochemistry and petrogenesis of the late Palaeoproterozoic A-type granites from the Dunhuang block, SE Tarim Craton, China: Implications for the break-up of the Columbia supercontinent. *Geological Magazine*, 151(4): 629~648.
- Zhang Chuanlin, Li Huikun, Santosh M, Li Zhengxiang, Zou Haibo, Wang Hongyan, Ye Haimin. 2012. Precambrian evolution and cratonization of the Tarim Block, NW China;

petrology, geochemistry, Nd-isotopes and U-Pb zircon geochronology from Archaean gabbro-TTG-potassic granite suite and Paleoproterozoic metamorphic belt. *Journal of Asian Earth Sciences*, 47: 5~20.

Zhang Chuanlin, Li Xianhua, Li Zhengxiang, Lu Songnian, Ye Haimin, Li Huimin. 2007. Neoproterozoic ultramafic-mafic-carbonatite complex and granitoids in Quruqtagh of northeastern Tarim Block, western China: geochronology, geochemistry and tectonic implications. *Precambrian Research*, 152(3~4): 149~169.

Zhang Chuanlin, Li Zhengxiang, Li Xianhua, Ye Haimin, Wang Aiguo, Guo Kunyi. 2006. Neoproterozoic bimodal intrusive complex in the Southwestern Tarim Block, Northwest China: age, geochemistry, and implications for the rifting of Rodinia. *International Geology Review*, 48: 112~128.

Zhang Chuanlin, Zou Haibo, Li Huikun, Wang Hongyan. 2013. Tectonic framework and evolution of the Tarim Block in NW China. *Gondwana Research*, 23(4): 1306~1315.

Zhao Guochun, Cawood P. 2012. Precambrian geology of Chinia. *Precambrian Research*, 222~223: 13~54.

Zhao Guochun, Sun Min, Wilde S A, Li Sanzhong. 2003. Assembly, Accretion and Breakup of the Paleo-Mesoproterozoic Columbia Supercontinent: Records in the North China Craton. *Gondwana Research*, 6: 417~434.

Zhu Wenbin, Zhang Zhiyong, Shu Liangshu, Lu Huafu, Su Jinbo, Yang Wei. 2008. SHRIMP U-Pb zircon geochronology of Neoproterozoic Korla mafic dykes in the northern Tarim Block, NW China: implications for the long-lasting breakup process of Rodinia. *Journal of the Geological Society, London*, 165: 887~890.

Zong Keqing, Klemd R, Yuan Yu, He Zhenyu, Guo Jingliang, Shi Xiaoli, Liu Yongsheng, Hu Zhaochu, Zhang Zeming. 2017. The assembly of Rodinia: The correlation of early Neoproterozoic (ca. 900 Ma) high-grade metamorphism and continental arc formation in the southern Beishan Orogen, southern Central Asian Orogenic Belt (CAOB). *Precambrian Research*, 290: 32~48.

Zuza A V, Yin An. 2017. Balkatach hypothesis: A new model for the evolution of the Pacific, Tethyan, and Paleo-Asian oceanic domains. *Geosphere*, 13: 1664~1712.

## 参 考 文 献

- 陈新跃, 王岳军, 孙林华, 范蔚茗. 2009. 天山冰达坂和拉尔敦达坂花岗片麻岩 SHRIMP 锆石年代学特征及其地质意义. *地球化学*, 38(5): 424~431.
- 陈义兵, 胡靄琴, 张国新, 张前锋. 1999. 西天山前寒武纪天窗花岗片麻岩的锆石 U-Pb 年龄及 Nd-Sr 同位素特征. *地球化学*, 28(6): 515~520.
- 陈义兵, 胡靄琴, 张国新, 张前锋. 2000. 西南天山前寒武纪基底时代和特征: 锆石 U-Pb 年龄和 Nd-Sr 同位素组成. *岩石学报*, 16(1): 91~98.
- 邓兴梁, 舒良树, 朱文斌, 马东升, 王博. 2008. 新疆兴地断裂带前寒武纪构造-岩浆-变形作用特征及其年龄. *岩石学报*, 24(12): 2800~2808.
- 胡靄琴, 韦刚健. 2006. 塔里木盆地北缘新太古代辛格尔灰色片麻岩形成时代问题. *地质学报*, 80: 126~134.
- 胡靄琴, 韦刚健, 江博明, 张积斌, 邓文峰, 陈林丽. 2010. 天山 0.9Ga 新元古代花岗岩 SHRIMP 锆石 U-Pb 年龄及其构造意义. *地球化学*, 39(3): 197~212.
- 李婷, 李智佩, 白建科, 李晓英. 2015. 伊犁地块达根别里新元古代花岗岩的锆石年代学、地球化学及其地质意义. *西北地质*, 48(3): 96~111.
- 李曰俊, 孙龙德, 胡世玲, 宋文杰, 王国林, 谭泽金. 2003. 塔里木盆地塔参 1 井底部花岗闪长岩的  $^{40}\text{Ar}$ - $^{39}\text{Ar}$  年代学研究. *岩石学报*, 19(3): 530~536.
- 刘颖, 刘海臣, 李献华. 1996. 用 ICP-MS 准确测定岩石样品中的 40 余种微量元素. *地球化学*, 25: 552~558.
- 莫宣学, 董国臣, 赵志丹, 周肃, 王亮亮, 邱瑞照, 张风琴. 2005. 西藏冈底斯带花岗岩的时空分布特征及地壳生长演化信息. *高校地质学报*, 11(3): 281~290.
- 邱检生, 王睿强, 赵蛟龙, 喻思斌. 2015. 冈底斯中段侏罗世辉长岩-花岗岩杂岩体成因及其对新特提斯构造演化的启示: 以日喀则东嘎岩体为例. *岩石学报*, 31(12): 3569~3580.
- 舒良树, 夏飞雅克, 马瑞士. 1998. 中天山北缘大型右旋走滑韧剪带研究. *新疆地质*, 16(4): 326~336.
- 孙晓猛, 王璞珺, 刘鹏举, 郝福江. 2006. 兴地断裂构造特征及其演化历史. *新疆地质*, 24(4): 348~352.

# The initial assembly of the Chinese Central Tianshan, Yili and Tarim blocks to the Rodinia supercontinent prior to the Early Neoproterozoic?

CAI Zhihui, MA Xuxuan, HE Bizhu

*Key Laboratory of Deep-Earth Dynamics of Ministry of Natural Resource, Institute of Geology,*

*Chinese Academy of Geological Sciences, Beijing, 100037*

\* Corresponding author: cai-zhihui@hotmail.com

## Abstract

The main Chinese blocks has been long thought to assemble to the Rodinia supercontinent later than other blocks around the globe. In the present study, we selected the Chinese Central Tianshan, Yili and Tarim blocks to test this hypothesis. We systematically analyzed the deformation and magma characteristics in the early Neoproterozoic (1.0–0.8 Ga). The lineation of the Neoproterozoic deformed rocks is nearly parallel to the trend of the orogenic belt, reflecting an intra-continental strike-slip shearing in the post-orogeny. The 1.0–0.8 Ga magmatic rocks are small-scale granites, no mafic enclaves, no or minor hornblendes in the mineral assemblage, showing high-K calc-alkaline affinity and peraluminous characteristics, with abundant inherited zircons, with the melting of lower crust as the main source and falling into post-collisional setting. The Ti-in-zircon and Zr-in-whole-rock geothermometers yield high crystallization temperatures (ca. 800°C) for these plutons. In combination with regional geology, we suggest that ① the Chinese Central Tianshan, Yili and Tarim blocks (belonging to the Greater Tarim Block) had been located in the interior of the Rodinia supercontinent and finished the collisional processes with other blocks during early Neoproterozoic, The deformation and magmatic records of 1.0–0.8 Ga reflect a tectonic event after continental collision. ② The high magmatic temperature can be explained as the thermal blanket effect from the supercontinent assembly. ③ The time of the initial assembly of the Greater Tarim Block (Chinese Central Tianshan, Yili and the present Tarim blocks) to the Rodinia supercontinent is prior to the Early Neoproterozoic (>1.0 Ga).

**Key words:** Neoproterozoic; Rodinia; Chinese Central Tianshan; Yili; Tarim